IEEE Access
Multidisciplinary | Rapid Review | Open Access Journal

Received April 12, 2019, accepted May 5, 2019, date of publication May 27, 2019, date of current version June 10, 2019.

Digital Object Identifier 10.1109/ACCESS.2019.2919099

Coverage, Capacity, and Error Rate Analysis of Multi-Hop Millimeter-Wave Decode and Forward Relaying

KHAGENDRA BELBASE, (Student Member, IEEE), CHINTHA TELLAMBURA, (Fellow, IEEE), AND HAI JIANG, (Senior Member, IEEE)
Department of Electrical and Computer Engineering, University of Alberta, Edmonton, AB T6G 1H9, Canada
Corresponding author: Khagendra Belbase (belbase@ualberta.ca)

ABSTRACT In this paper, we analyze the end-to-end (e2e) performance of a millimeter-wave (mmWave) multi-hop relay network. The relays in it are decode-and-forward (DF) type. As appropriate for mmWave bands, we incorporate path loss and blockages considering the links to be either line of sight (LOS) or non line of sight (NLOS). The links also experience Nakagami-m fading with different m-parameters for the LOS and NLOS states. We consider two scenarios, namely sparse and dense deployments. In the sparse case, the nodes (relays and the destination) are limited by additive noise only. We derive closed-form expressions for the distribution of equivalent e2e signal-to-noise-ratio (SNR), coverage probability, ergodic capacity, and symbol error rate (SER) for the three classes of digital modulation schemes, namely, binary phase shift keying (BPSK), differential BPSK (DBPSK), and square-quadrature amplitude modulation (QAM). In the dense case, the nodes are limited by interference only. Here, we consider two situations: 1) interference powers are independent and identically distributed (i.i.d.) and 2) they are independent but not identically distributed (i.n.i.d.). For the latter situation, closed-form analysis is exceedingly difficult. Therefore, we use the *Welch–Satterthwaite Approximation* for the sum of Gamma variables to derive the distribution of the total interference. For both situations, we derive the distribution of signal-to-interference ratio (SIR), coverage probability, ergodic capacity, and SERs for the DBPSK and BPSK. We study how these measures are affected by the number of hops. The accuracy of the analytical results is verified via Monte-Carlo simulation. We show that multi-hop relaying provides significant coverage improvements in blockage-prone mmWave networks.

INDEX TERMS 5G, blockage, mmWave communication, multi-hop network, relay.

I. INTRODUCTION

Rapid and continuous growth of data services over wireless networks has been expected for the near future; for example, the worldwide mobile data volume will increase five folds from 2018 to 2024, reaching 136 Exabytes per month [1]. The growth drivers include data-hungry mobile applications, high-definition video, virtual reality applications, and a massive number of Internet of things (IoT) devices connected to fifth generation (5G) networks. To meet this growth, more wireless spectrum is needed, which is available in abundance in millimeter-wave (mmWave) bands (20-100 GHz). Their use is thus motivated by three fundamental factors: i) congestion and limited bandwidth availability in sub-6 GHz bands, ii) the saturation of spectral efficiency of current systems leaving little room for improvement, and iii) the potential of mmWave bandwidths to deliver Gbps data rates.

But there is no free lunch. High path losses, blockages by obstacles (human bodies, buildings, vehicles and others) and poor signal diffraction properties are challenges [2]. For example, 28 GHz mmWave signals suffer 28 dB and 40 dB attenuations due to a 185 cm brick wall and 3.8 cm thick tinted glass, respectively [3]. Such high attenuation levels yield poor coverage in indoor areas, in outdoor areas blocked by buildings and in the non-line-of-sight (NLOS) regions even for short communication distances [4].

These problems can be mitigated by the use of wireless relays. They can extend the cellular radio range, improve the cell-edge user experience, combat shadowing and reduce infrastructure deployment costs in mmWave networks [3].

The associate editor coordinating the review of this manuscript and approving it for publication was Irfan Ahmed.

For example, in lognormal shadowing, randomly located amplify-and-forward (AF) relays improve coverage and spectral efficiency [5], and two-way AF relay networks perform likewise [6]. Relay selection can also yield performance gains. For instance, the selection of a relay that provides minimum path loss to the receiver improves the coverage of a mmWave decode-and-forward (DF) relay [7]. Optimal placement of a relay using unmanned autonomous vehicles can overcome the blockages and enable faster connectivity in mmWave networks [8]. Both the ground reflected signal and LOS signals can be used for relaying, and beamwidth and self interference affect the achievable rate [9]. These works demonstrate the ability of relaying to overcome blockages and improve the rate and coverage of mmWave networks.

Multi-hop relaying comprises of one or more relays placed between the source and destination, which breaks the link into two or more short links (hops), improving the network coverage as well as the end-to-end transmission rate. Line-of-sight (LOS) conditions can be obtained by carefully planning the relay positions, thus improving the data rates. If relay nodes are fairly densely deployed, then the source and destination nodes can be fairly close to one or more relays. Moreover, the major limitation of mmWave is not necessarily the high path loss per se, rather the attenuation due to the blockages because of high penetration loss and poor signal diffraction at mmWave frequencies [10]. Fortunately, the use of multiple hops may mitigate them as these impairments decrease with the reduction of transmission distance. Therefore, seamless coverage in blocked and indoor areas is possible [4].

A. PERFORMANCE ANALYSIS OF MULTI-HOP RELAYS IN SUB- 6 GHz NETWORKS

Multi-hop relaying alleviates outage in conventional networks in sub-6 GHz bands [11], [12]. For example, reference [11] analyzes the end-to-end (e2e) outage probability of a multi-hop network. In [12], the authors present an analysis of a multi-hop AF network consisting of a source, a number of relays and a destination, in which the relays and destination are impaired by a fixed number of co-channel interferers. In [13], the authors analyze the outage probability and symbol error rates (SERs) in a multi-hop network perturbed by Poisson distributed co-channel interferers, taking into account the distance dependent path loss in signal and interference power. Many multi-hop studies demonstrate improved performances [14]–[18].

B. PERFORMANCE ANALYSIS OF mmWave MULTI-HOP NETWORKS

Although multi-hop mmWave relaying has been studied [19]–[26], all of them except [26] focus on the upper layers (medium access control and network layers). For example, in [19], a directional medium access control protocol is provided to select a relay for data forwarding using multi-hop path. Routing protocols for device-to-device multi-hop systems are proposed in [20] for transmitting video. In [21], dynamic traffic is scheduled for self backhaul networks. Reference [22] proposes a dynamic duplex resource allocation for uplink and downlink transmissions given concurrent co-channel transmissions. All these works show that multi-hop links improve coverage and rate significantly in mmWave networks. For instance, the work in [24] optimizes the performance of large-scale mmWave backhaul networks for multiple mobile network operators. A self-organizing mmWave backhaul link can be established with existing LTE (Long Term Evolution) dual connectivity techniques [25]. Moreover, multi-hop relaying also significantly improves connectivity in mmWave networks affected by random blockages [23].

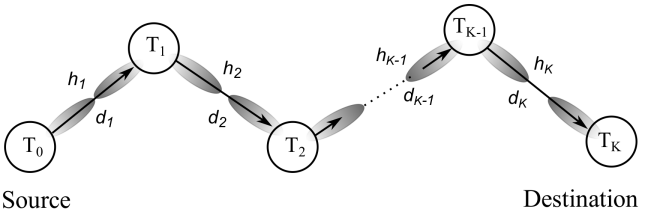

FIGURE 1. A multi-hop wireless relay network.

Among all the above works, only the work in [26] investigates the multi-hop relay physical layer performance in terms of bit error probability (BEP). This work considers AF relays, and derives exact BEP expressions for two modulation schemes, as well as a tight lower bound of BEP. The diversity and the coding gains are also analyzed. In addition, the power allocation is optimized to minimize BEP. In contrast, our paper focuses on DF relays and thus takes a radically different analytical approach. Our paper does not attempt the power optimization and investigates both sparse and dense mmWave scenarios whereas the work [26] focuses on the dense scenario only. We also derive other performance measures, namely, coverage probability, ergodic capacity, and SER. In addition, all the previous works omit NLOS scenarios, which however are common for mmWave links [2], [27]. We consider both LOS and NLOS links in this paper.

C. PROBLEM STATEMENT AND CONTRIBUTIONS

Hence, the works in [19]–[24] and other previous mmWave multi-hop contributions have not provided a general, comprehensive analysis of system performance and quality of service (QoS) parameters from the end user perspective. Such an analysis is important for both design and innovation purposes of mmWave networks and for the advancement of wireless research. To fill this missing link, we analyze the e2e performance of a multi-hop mmWave network (Fig. 1) by fully considering mmWave specific impairments such as blockages and path losses and small-scale fading. Blockages are considered by allowing each link to be in either LOS or NLOS state with a certain probability that depends on the density and size of the blocking objects and the length of the link. The specific contributions are as follows:

1) We first consider a sparse deployment scenario. The mmWave multi-hop network is then noise limited, and

each hop can be in either LOS or NLOS state. We derive the closed-from distribution of e2e signal to noise ratio (SNR) given the DF relays. This is a general result that is applicable to any combination of link states, and special cases such as all links being LOS can be easily evaluated.

2) We also derive the destination coverage probability via complementary cumulative distribution function (CCDF). Moreover, rate coverage probability, ergodic capacity and symbol error rate (SER) for three classes of digital modulation schemes, namely, binary phase shift keying (BPSK), differential BPSK (DBPSK), and square-quadrature amplitude modulation (QAM) are derived. These modulations are widely used in existing 60 GHz systems, such as 802.11ad, IEEE 802.15.3c and ECMA-387, and are expected to be used in future mmWave standards [3].
3) Next, for dense relay deployment scenarios (interference-limited case), we derive the distribution of signal-to-interference-ratios (SIRs) at the relays and destination. The SIR of each relay has Beta Prime distribution when interference signals are independent and identically Gamma distributed (i.i.d.). However, when they are independent but not identically distributed (i.n.i.d.), the distribution of sum of interference powers is extremely complicated. To overcome this challenge, we use a classical Welch-Satterthwaite approximation for the sum of Gamma variables [28], [29]. We derive the CCDFs of the SIRs at the relays and destination.
4) However, the analysis of ergodic capacity and SER when relay SIRs are i.n.i.d. is not tractable. Therefore, considering identical SIRs at all relays, we derive the closed-form expressions for ergodic capacity and SER. Due to the high complexity of exact ergodic capacity expressions, we also derive high SNR approximate capacity expressions.
5) We provide extensive simulation results to verify our derivations and to draw broad conclusions on the performance of mmWave multi-hop links.

The paper is organized as follows. Section II presents the system model. In Section III, the major performance metric, coverage probability is derived for the noise limited multi-hop system by deriving the closed form expressions for the CCDF of e2e SNR. Analysis of ergodic capacity and SER are derived at the end of Section III. Section IV derives the coverage probabilities in interference limited scenario together with ergodic capacity and SER.[1] Section V presents the numerical results and Section VI presents the conclusion.

Notations: for random variable (r.v.) X, $F_X(\cdot)$, $\tilde{F}_X(\cdot)$ and $f_X(\cdot)$ represent cumulative distribution function (CDF), CCDF and probability density function (PDF), respectively. $\mathbb{P}(\cdot)$ and $\mathbb{E}[\cdot]$ denote probability and expectation. $\mathcal{G}(\alpha, \lambda)$ denotes a Gamma distribution with PDF $f(x) = \frac{\lambda^\alpha}{\Gamma(\alpha)} x^{\alpha-1} e^{-\lambda x}$, $x > 0$ where $\lambda > 0$ and $\alpha \geq 1$ are the rate and shape parameters, respectively, and $\Gamma(z) = \int_0^\infty x^{z-1} \mathrm{e}^{-x} dx$ is the Gamma function.

[1] Noise limited scenario and interference limited scenario are typical scenarios in mmWave analysis. Further details on when these scenarios arise and the transitional behavior of mmWave network from noise-limited to interference-limited regime can be found in [30].

II. SYSTEM MODEL

A. NETWORK MODELING

We consider a multi-hop mmWave wireless network with one source (T_0), one destination (T_K), and $K-1$ intermediate relays so that the total number of hops in the system is K (Fig. 1). We assume that each node operates at a mmWave band and is capable of directional beamforming [31], which is a technique to point antenna transmit and receive beams in the desired direction and can be performed using analog, digital, and hybrid methods [3]. Node T_k ($k = 0, \ldots, K-1$) transmits with power $\mathcal{P}_k$, the distance between T_{k-1} and T_k ($k = 1, \ldots, K$) is d_k, and G_k is the beamforming gain of T_k. The small-scale fading coefficient of the k-th hop channel is denoted by h_k.

We consider DF relays where each relay decodes the received message, re-encodes it and retransmits it to the next relay until the message reaches the destination. Due to the decoding by each relay, additive noise is not accumulated, which improves the performance compared to that of AF relays. However, decoding error propagation is a potential problem [32].

B. PATH LOSS MODELING

Path loss can be represented as a function of the propagation distance from the transmitter to the receiver and the operating frequency [10]. Here we use a simple but common model with the path loss being d^{ν_l} where d is the distance and $\nu_l \geq 2$ is a path loss exponent (PLE) and the subscript $l \in \{L, N\}$ denotes LOS and NLOS link conditions which have distinct PLEs [2]. The typical values of $\nu_L = 2$ and $\nu_N = 3.3$ are used in this study. With higher PLE values, NLOS links are weaker compared to LOS links; however, they make communication possible because of the significant power from reflected and scattered components at mmWave frequencies [2]. Therefore, we consider that each link can be in either LOS or NLOS state. In practice, careful planning may increase the LOS probability by the placement of the relays to minimize blockages.

C. DIRECTIONAL BEAMFORMING MODELING

We approximate the antenna gain pattern with the simplified two-sector model [27], where the main lobe and side lobe gains are $G_{\max}$ and $G_{\min}$. With half-power beamwidth of ϕ, beamforming gain as a function of azimuth angle φ is

$$G(\varphi) = \begin{cases} G_{\max} & \text{if } |\varphi| \leq \frac{\phi}{2} \\ G_{\min} & \text{otherwise.} \end{cases}$$

The typical values of $G_{\max} = 18$ dBi and $G_{\min} = -2$ dBi are used in our study. These gains depend on the number of elements and their geometry in antenna array, and are

achievable by simple analog beamforming [33]. We assume perfect beam alignment between the transmitting and receiving nodes (T_{k-1} and T_k), so that the overall link gain is $G_{\text{eq}} \triangleq G_{\max}^2$. Nevertheless, beam misalignment errors, which are out of the scope of this paper, can be a topic of future research.

D. BLOCKAGE MODELING

Obstacles (building, vehicles and other objects) in the direct link may block the transmitter-receiver link, making it NLOS. This increases the path loss significantly compared to that of an LOS link. Therefore, blockage inclusion is crucial for realistic performance analyses [34]. To model mmWave blockages, the work in [34] has proposed a geometric stochastic model via the random shape theory. It assumes that obstacles are spatially distributed as a homogeneous Poisson point process (PPP) and their shape, size, and orientation are randomly chosen from a predefined set. With this model, a link of length d will be in LOS or NLOS state with $e^{-\beta d}$ or $1-e^{-\beta d}$ probability, where β is the blockage parameter [34]. This model may accurately describe a real deployment scenario if β is chosen to match the expected length and width of the obstacles:

$$\beta = \frac{2\eta\left(\mathbb{E}[L]+\mathbb{E}[W]\right)}{\pi},$$

where the blockage density η is the number of blocking obstacles or buildings per unit area, and $\mathbb{E}[L]$ and $\mathbb{E}[W]$ are average length and width of the objects. Alternatively, the works in [27], [35] propose a fixed ball LOS model, where an area within a fixed radius from a transmitter is considered to be in LOS with a fixed probability. However, we use the above exponential model, which provides more tractability in multi-hop performance analysis than approximated LOS ball models [27], [35].

E. SMALL-SCALE FADING

Empirical results show that mmWave channel exhibits multipath characteristics, especially in NLOS links, leading to small-scale channel fading [2]. However, in an LOS link, the direct path dominates the relatively small multi-path contribution. Thus, to correctly represent the LOS and NLOS links, we model the small-scale fading coefficient h_l, $l \in \{L, N\}$ as Nakagami-m distributed with different m-parameters for LOS and NLOS as m_L and m_N, respectively [27]. To represent the relative degrees of multipath in these two cases, we use $m_L \gg m_N$. The corresponding fading power gain $|h_l|^2$ is distributed $\mathcal{G}(m_l, m_l)$.

F. RECEIVED SIGNAL MODEL

With the described system model and mmWave specific propagation assumptions, average received signal power at T_k is given by

$$Q_{k,l} = \frac{\mathcal{P}_{k-1}\Psi_k\mathbb{E}\left[|h_{k,l}|^2\right]}{d_k^{v_l}} \tag{1}$$

where $\mathcal{P}_{k-1}$ is the transmit power of T_{k-1}, $\Psi_k = G_{k-1}G_k\left(\frac{c}{4\pi f}\right)^2$ is a constant where G_k and G_{k-1} are the beamforming gains at T_{k-1} and T_k respectively, c is the speed of light in free space and f is the operating frequency, $h_{k,l}$, $l \in \{L, N\}$ is the normalized small-scale fading amplitude of the k-th ($k = 1, \ldots, K$) link which follows Nakagami-m distribution with parameter m_l, $\mathbb{E}\left[|h_{k,l}|^2\right]$, $l \in \{L, N\}$ is the average fading power, d_k is the distance between T_{k-1} and T_k, and v_l, $l \in \{L, N\}$ is the path loss exponent, where L and N denote LOS and NLOS link conditions, respectively.

III. PERFORMANCE OF NOISE LIMITED NETWORK

The noise-limited case can occur due to sparse deployment of mmWave nodes. For this case, we derive SNR coverage probability, rate coverage, ergodic capacity, and symbol error rate (where the noise power is dominant and interference is negligible). The received signal at T_k can then be written as

$$y_{k,l} = \sqrt{Q_{k,l}}\, h_{k,l}\, x_{k-1} + w_k \tag{2}$$

where x_{k-1} is the transmitted symbol from T_{k-1} and w_k is the zero mean Gaussian noise with power N_0 at the input of T_k. Considering all these factors, we can write the received SNR at node k ($k = 1, 2, \ldots, K$) as

$$\gamma_k = \bar{\gamma} X_k \tag{3}$$

where $\bar{\gamma}$ is an average SNR constant applicable to each hop and X_k is a Gamma r.v. whose parameters depend on LOS or NLOS state of the hop. With this model, we derive the e2e SNR of the multi-hop network. However, before that, we present two necessary lemmas, which will subsequently help us to derive the distribution of the e2e SNR.

Lemma 1: The CCDF of $X_{\min} = \min\{X_1, X_2, \cdots, X_K\}$ *where* $X_k \sim \mathcal{G}(1, \lambda_k)$, $k = 1, \ldots, K$, *are independently distributed is given by*

$$\tilde{F}_{X_{\min}}(x) = e^{-(\lambda_1+\cdots+\lambda_K)x}, \quad 0 \le x < \infty. \tag{4}$$

Proof: All the X_k's are independent Exponential r.v.s with the $\tilde{F}_{X_k}(x) = e^{-\lambda_k x}$. Since $\tilde{F}_{X_{\min}}(x) = \prod_k \tilde{F}_{X_k}(x)$, the lemma follows immediately. ∎

Lemma 1 is sufficient to describe independent Rayleigh-fading hops only. More generally, Lemma 2 applies for independent Nakagami-fading hops.

Lemma 2: The CCDF of $X_{\min} = \min\{X_1, X_2, \cdots, X_K\}$ *where* $X_k \sim \mathcal{G}(\alpha_k, \lambda_k)$, $k = 1, \ldots, K$, *are independently distributed is given by*

$$\tilde{F}_{X_{\min}}(x) = e^{-(\lambda_1+\cdots+\lambda_K)x}\sum_{m=0}^{\hat{k}}\mu_m x^m \quad 0 \le x < \infty \tag{5}$$

where $\hat{k} = \sum_k \alpha_k - K$ *and* $\mu_m = \prod_{\sum n_k = m}\frac{(\lambda_k)^{n_k}}{n_k!}$, $m = 0, 1, \ldots, \hat{k}$.

Proof: See Appendix A. ∎

We will next use Lemmas 1 and 2 to derive the distribution of e2e SNRs.

A. DISTRIBUTION OF e2e SNR

In a DF multi-hop link, independent outages occur in each hop, and the overall e2e outage is dominated by the weakest link [11]. Therefore, the CCDF of equivalent e2e SNR, denoted as γ_{eq}, can be written as

$$\begin{aligned}\tilde{F}_{\gamma_{\text{eq}}}(x) &= \mathbb{P}\left(\min(\bar{\gamma}X_1, \ldots, \bar{\gamma}X_K) > x\right) \\ &= \mathbb{P}\left(\bar{\gamma}\min(X_1, \ldots, X_K) > x\right), \end{aligned} \tag{6}$$

where each X_k, $k = 1, \cdots, K$ can have one of the two statistical distributions due to the k-th link being in LOS or NLOS condition. In the following, for convenience, we assume that the probability of each hop being in LOS or NLOS state is identical for all hops. This describes a spatially homogeneous blockage distribution. Accordingly, for each hop, we denote the probability of LOS state as p, and the probability of NLOS state as q with $p + q = 1$.

Theorem 1: The CCDF of equivalent e2e SNR in a multi-hop network when the k-th hop SNRs ($k = 1, \ldots, K$) are independently distributed as $\mathcal{G}(1, \lambda_k^{s_k})$ is given by

$$\tilde{F}_{\gamma_{\text{eq}}}(x) = \sum_{\mathbf{s}} p^{w(\mathbf{s})} q^{K-w(\mathbf{s})} e^{\frac{-\Lambda_{\mathbf{s}} x}{\bar{\gamma}}}, \quad 0 \le x < \infty, \tag{7}$$

where $w(\mathbf{s})$ is the Hamming weight of state $\mathbf{s} = [s_1, \cdots, s_K]$ where $s_k \in \{0, 1\}$ denotes if k-th hop is LOS ($s_k = 1$) or NLOS ($s_k = 0$). State $\mathbf{s}$ will take 2^K distinct values, and $\Lambda_{\mathbf{s}} = \lambda_1^{s_1} + \cdots + \lambda_K^{s_K}$.

Proof: We start with (6) and illustrate the proof by an example. For example, if $K = 3$, then $\mathbf{s} \in [000, 001, 010, \ldots]$. If $\mathbf{s} = 010$, the first and third hops are NLOS and the second hop is LOS. The probability of this state is pq^2. In this state, the three hop SNRs will be exponential with parameters λ_1^0, λ_2^1 and λ_3^0, respectively. By applying Lemma 1, the CCDF of the minimum SNR is $e^{-(\lambda_1^0+\lambda_2^1+\lambda_3^0)x/\bar{\gamma}}$. The same process applies to all the other states. Finally, we weigh these CCDFs by their probabilities and sum up over all possible link states $\mathbf{s}$, and then we obtain (7). ∎

Theorem 1 provides the coverage probability for independent Rayleigh fading hops, i.e., all hop SNRs are exponentially distributed. Incidentally, this is the most common fading model used for sub-6 GHz multi-hop networks.

Theorem 2: The CCDF of equivalent e2e SNR in a multi-hop network when k-th hop SNR are independently distributed as $\mathcal{G}(\alpha_k^{s_k}, \lambda_k^{s_k})$ is given by

$$\tilde{F}_{\gamma_{\text{eq}}}(x) = \sum_{\mathbf{s}} p^{w(\mathbf{s})} q^{K-w(\mathbf{s})} e^{-\frac{\Lambda_{\mathbf{s}} x}{\bar{\gamma}}} \sum_{m=0}^{\hat{k}} \mu_m^{\mathbf{s}} \left(\frac{x}{\bar{\gamma}}\right)^m \tag{8}$$

where $\mu_m^{\mathbf{s}}$ are obtained from Lemma 2, in which the superscript $\mathbf{s}$ denotes one of the states of the K-hop system.

Proof: The proof is similar to that of Theorem 1 and is omitted. Note that, in this case k-th hop parameters $\alpha_k^{s_k}$ and $\lambda_k^{s_k}$ are chosen according to LOS or NLOS condition. ∎

Theorem 2 provides the distribution of e2e SNR for independent Nakagami-m hops and helps us to analyze coverage, capacity and error rates of the network (Fig. 1). Before proceeding to these analysis, we use Theorem 2 to derive the PDF of e2e SNR in Proposition 1.

Proposition 1: The PDF of the equivalent e2e SNR can be written as

$$\begin{aligned} f_{\gamma_{\text{eq}}}(x) = \sum_{\mathbf{s}} p^{w(\mathbf{s})} q^{K-w(\mathbf{s})} \left(\frac{1}{\bar{\gamma}}\right) \mathrm{e}^{-\frac{\Lambda_{\mathbf{s}} x}{\bar{\gamma}}} \\ \times \left(\Lambda_{\mathbf{s}} \sum_{m=0}^{\hat{k}} \mu_m^{\mathbf{s}} \left(\frac{x}{\bar{\gamma}}\right)^m - \sum_{m=1}^{\hat{k}} m\mu_m^{\mathbf{s}} \left(\frac{x}{\bar{\gamma}}\right)^{m-1}\right). \end{aligned} \tag{9}$$

Proof: The PDF in (9) follows by differentiating $\tilde{F}_{\gamma_{\text{eq}}}(x)$ given in (8). ∎

With the closed-form PDF in Proposition 1, we derive the performance measures such as ergodic capacity and SER below.

B. SNR COVERAGE PROBABILITY

SNR coverage is the probability that the destination SNR is larger than a predefined threshold, γ_{th}.

Proposition 2: The SNR coverage probability of the noise-limited mmWave multi-hop DF link is given by

$$P_{\text{cov}} = \sum_{\mathbf{s}} p^{w(\mathbf{s})} q^{K-w(\mathbf{s})} e^{-\frac{\Lambda_{\mathbf{s}}\gamma_{\text{th}}}{\bar{\gamma}}} \sum_{m=0}^{\hat{k}} \mu_m^{\mathbf{s}} \left(\frac{\gamma_{\text{th}}}{\bar{\gamma}}\right)^m. \tag{10}$$

Proof: By definition, coverage probability is the CCDF of the e2e SNR at γ_{th}, which is obtained from (8) with $x = \gamma_{\text{th}}$. ∎

P_{cov} in Proposition (2) provides a quantitative measure on the quality of service and may help network designs. For example, if $P_{\text{cov}} = 0.8$ at $\gamma_{\text{th}} = 10$ dB, SNR is at least 10 dB for 80% of the time. Thus, link parameters may be fine tuned based on the service quality requirements.

C. RATE COVERAGE PROBABILITY

Rate coverage is the probability that the achievable transmission rate exceeds a predefined threshold $R_{\text{th}} > 0$. Clearly, the number of data bits received per second is an important metric to gauge the link performance. Moreover, since the use of mmWave bands initially targets high transmission rates, rate coverage is a highly relevant performance measure for mmWave communications.

In mmWave networks, large path losses make signal propagation beyond the nearest node highly difficult. With this condition, alternately located relays can co-transmit to their corresponding receiving nodes during the same time slot without causing any significant interference to other nodes [19]. Therefore, $K/2$ simultaneous transmissions can occur when the number of hops K is even or alternatively $(K + 1)/2$ and $(K - 1)/2$ simultaneous transmissions can occur when K is odd. To this end, the achievable rate for the multi-hop relay network can be written as

$$R = \frac{W}{2} \log_2\left(1 + \gamma_{\text{eq}}\right) \text{ bits per second} \tag{11}$$

where W is the bandwidth assigned to the typical user and the factor of $1/2$ is used because the network can equivalently transmit one symbol per two time slots.

Corollary 1: The rate coverage probability of a multi-hop relay transmission is given by

$$P_{\text{cov}}^{\text{Rate}} = \sum_{\mathbf{s}} p^{w(\mathbf{s})} q^{K-w(\mathbf{s})} e^{-\frac{\Lambda_{\mathbf{s}}\mathcal{C}}{\bar{\gamma}}} \sum_{m=0}^{\hat{k}} \mu_m^{\mathbf{s}} \left(\frac{\mathcal{C}}{\bar{\gamma}}\right)^m \tag{12}$$

where $\mathcal{C} = 2^{\frac{2R_{\text{th}}}{W}} - 1$.

Proof: By manipulating (11), we find $\mathbb{P}(R > R_{\text{th}}) = \mathbb{P}(\gamma_{\text{eq}} \geq \mathcal{C})$. ■

Using (12), we can compute the probability of achieving a given minimum data rate at the receiver, which justifies the use of mmWave in multi-hop relaying as the major motive is to achieve higher data rate. In addition, system parameters such as transmit power, beamforming gain, and number of hops can be adjusted to achieve a required rate via (12).

D. ERGODIC CAPACITY

To compute the e2e ergodic capacity, similar to Section III-C, we assume that alternate relays (T_k and T_{k+2}) can co-transmit in the same time-frequency slot without causing significant mutual interference [19]. With this setup, a multiplexing gain of $1/2$ can be achieved irrespective of the number of hops. The subsequent capacity expressions are stated accordingly.

Theorem 3: For a multi-hop mmWave DF relay network, ergodic capacity (bps/Hz) is given by

$$\tilde{C} = \frac{1}{2\ln 2} \sum_{\mathbf{s}} p^{w(\mathbf{s})} q^{K-w(\mathbf{s})} \mathrm{e}^{\frac{\Lambda_{\mathbf{s}}}{\bar{\gamma}}} \Bigg[\mu_0^{\mathbf{s}} \Gamma\left(0, \frac{\Lambda_{\mathbf{s}}}{\bar{\gamma}}\right) + \sum_{m=1}^{\hat{k}} \frac{\mu_m^{\mathbf{s}}}{\bar{\gamma}^m} \Bigg((-1)^m \Gamma\left(0, \frac{\Lambda_{\mathbf{s}}}{\bar{\gamma}}\right) + \sum_{n=1}^{m} \binom{m}{n} \times (-1)^{m-n} \left(\frac{\bar{\gamma}}{\Lambda_{\mathbf{s}}}\right)^n \Gamma\left(n, \frac{\Lambda_{\mathbf{s}}}{\bar{\gamma}}\right) \Bigg) \Bigg], \tag{13}$$

where $\Gamma(x, a) = \int_a^\infty t^{x-1} \mathrm{e}^{-t} dt$ *is the upper incomplete gamma function.*

Proof: See Appendix B. ■

The expression (13) provides the capacity versus average per hop SNR of the multi-hop network and can be easily evaluated using MATLAB. Note that $\Gamma(0, z)$ is equivalent to exponential integral function $E_1(z)$ [36].

1) HIGH SNR CAPACITY APPROXIMATION

Simplification of the exact capacity expression (13) is desirable; for example, simpler high-SNR expressions can be extremely accurate and they allow the study of limiting performances. Therefore, the asymptotic capacity expression is derived next.

Corollary 2: At high SNR, i.e., $\bar{\gamma} \to \infty$, the ergodic channel capacity is given by

$$\tilde{C}_{\text{high SNR}} = \frac{1}{2\ln 2} \Bigg[\ln(\bar{\gamma}) + \sum_{\mathbf{s}} p^{w(\mathbf{s})} q^{K-w(\mathbf{s})} \times \Bigg(\sum_{m=0}^{\hat{k}} \frac{\mu_m^{\mathbf{s}} m!}{\Lambda_{\mathbf{s}}^m} \Big(\Psi(m+1) - \ln(\Lambda_{\mathbf{s}}) \Big) - \sum_{m=1}^{\hat{k}} \frac{\mu_m^{\mathbf{s}} m!}{\Lambda_{\mathbf{s}}^m} \Big(\Psi(m) - \ln(\Lambda_{\mathbf{s}}) \Big) \Bigg) \Bigg] \tag{14}$$

where $\Psi(z) = \frac{d(\ln \Gamma(z))}{dz}$ *is a Digamma function [37, 6.3.1].*

Proof: When $\bar{\gamma} \to \infty$, we have

$$\mathbb{E}[\ln(1 + \bar{\gamma} X)] \approx \ln(\bar{\gamma}) + \mathbb{E}[\ln X]. \tag{15}$$

For a r.v. $X > 0$, $\mathbb{E}[\ln X]$ is equal to the first derivative of the Mellin transform of X evaluated at $t = 1$. The Mellin transform of X is defined as

$$M_X(t) = \mathbb{E}\left[X^{t-1}\right] \tag{16}$$

where we have $X = \min\{X_1, \cdots, X_K\}$. Theorem 2 yields the PDF of X as

$$f_X(x) = \sum_{\mathbf{s}} p^{w(\mathbf{s})} q^{K-w(\mathbf{s})} \mathrm{e}^{-\Lambda_{\mathbf{s}} x} \times \left(\Lambda_{\mathbf{s}} \sum_{m=0}^{\hat{k}} \mu_m^{\mathbf{s}} x^m - \sum_{m=1}^{\hat{k}} m \mu_m^{\mathbf{s}} x^{m-1} \right). \tag{17}$$

Now, using the PDF (17) to compute the expectation in (16) results in

$$M_X(t) = \sum_{\mathbf{s}} p^{w(\mathbf{s})} q^{K-w(\mathbf{s})} \Bigg(\sum_{m=0}^{\hat{k}} \frac{\mu_m^{\mathbf{s}} \Gamma(m+t)}{\Lambda_{\mathbf{s}}^{(m+t-1)}} - \sum_{m=1}^{\hat{k}} \frac{m \mu_m^{\mathbf{s}} \Gamma(m+t-1)}{\Lambda_{\mathbf{s}}^{(m+t-1)}} \Bigg). \tag{18}$$

By differentiating (18) over t, substituting $t = 1$, and again substituting the resulting expression in (15), we have (14). ■

The asymptotic capacity in (14) is a function of $\bar{\gamma}$ and represents a straight line with slope $(2\ln(2))^{-1}$ and y-intercept that depends on the summation term in $\mathbf{s}$.

E. SER ANALYSIS

Symbol error occurs if the received symbol at destination differs from the transmitted symbol from the source. Thus, SER is the ratio of the number of erroneous symbols received to the total number of transmitted symbols. In a multi-hop network, error in any intermediate hop can cause the error at destination. Hence, the exact computation of SER in DF network needs to consider all possible errors of symbol being erroneously mapped to a different symbol in the given constellation and in each hop. This means that, for higher constellation size such as M-ary quadrature amplitude modulations (M-QAM), e2e SER computation is cumbersome due

to large number of possible mapping permutations and it gets complicated with the increased number of hops. Therefore, SER in a multi-hop networks is generally computed assuming that symbol error in any hop will contribute to the overall SER and without forward error correction at intermediate nodes [32], [38]. However, this approach can only provide an upper bound on the SER which is computed using per hop SER as follows

$$P_{\text{ub}} \leq \sum_{\mathbf{s}} p^{w(\mathbf{s})} q^{K-w(\mathbf{s})} \left(1 - \prod_{k=1}^{K} \left(1 - P_k^{s_k}\right)\right) \tag{19}$$

where $P_k^{s_k}$ is the SER in k-th hop having state $\mathbf{s}$ and (19) simply means that symbol error will occur if error occurs in any of the hops. In the following three propositions, we provide the k-th hop SER for three classes of modulation schemes, namely *noncoherent binary signaling, coherent binary signaling, and M-QAM*. For the notational simplicity, we omit the superscript s_k and simply write k-th hop SER as P_k and the Nakagami-m fading parameters as α_k and λ_k.

Proposition 3: For a class of noncoherent binary signaling, such as differential phase shift keying (DBPSK) and frequency shift keying (FSK), k-th hop SER is given by

$$P_k = a \left(\frac{\lambda_k}{\lambda_k + b\bar{\gamma}}\right)^{\alpha_k} \tag{20}$$

where α_k and λ_k are the fading parameters of k-th hop, and a and b are modulation specific constants, see [39, Table I]. For example, for DBPSK, we have $a = 0.5$ and $b = 1$.

Proof: In this case, SER conditioned on link SNR x can be written as $P_k(x) = a \exp(-bx)$. Now P_k can be computed by averaging $P_k(x)$ over the SNR PDF using

$$P_k = \int_0^{\infty} P_k(x) f_{\gamma_k}(x) dx, \tag{21}$$

where $f_{\gamma_k}(x) = \frac{1}{\Gamma(\alpha_k)} \left(\frac{\lambda_k}{\bar{\gamma}}\right)^{\alpha_k} x^{\alpha_k - 1} e^{-\frac{\lambda_k}{\bar{\gamma}} x}$. The integral can be simplified to (20) using [36, eq. 3.351.3]. ■

Since the noncoherent signaling schemes do not require the phase information for demodulation, implementation complexity decreases. This is highly desired in low complexity mmWave terminals. Next, we provide the SER for coherent binary signaling schemes in the following proposition.

Proposition 4: For a class of coherent binary signaling, such as binary phase shift keying (BPSK) and FSK, k-th hop SER is given by

$$P_k = \frac{a 2^{1-2\alpha_k} \Gamma(2\alpha_k)}{\Gamma(\alpha_k)\Gamma(\alpha_k + 1)} \left(\frac{\lambda_k}{b\bar{\gamma}}\right)^{\alpha_k} \times {}_2F_1\left(\alpha_k, \alpha_k + \frac{1}{2}; \alpha_k + 1; -\frac{\lambda_k}{b\bar{\gamma}}\right) \tag{22}$$

where α_k and λ_k are the fading parameters of k-th hop, a and b are constants depending on the modulation scheme [39] (for BPSK, $a = 0.5$ and $b = 1$), and ${}_2F_1(\cdot)$ is the Gaussian hypergeometric function defined in [37, eq.15.1.1].

Proof: In this case, conditional SER conditioned on link SNR x is given by $P_k(x) = a \operatorname{erfc}\left(\sqrt{bx}\right)$, where $\operatorname{erfc}(z) = \frac{2}{\sqrt{\pi}} \int_z^{\infty} e^{-t^2} dt$ is the complementary error function. Now (22) can be obtained by averaging $P_k(x)$ with SNR PDF using (21) and then solving the integral [40]. ■

Coherent BPSK maps one bit per symbol and requires the phase information for the demodulator. Although this increases demodulation complexity, the SER improves compared to DBPSK. Next, we provide the SER of multi-level modulations.

Proposition 5: In case of quadrature and multi-level signaling, such as QPSK, MSK, and Square-QAM modulations, k-th hop SER is given by

$$\begin{aligned} P_k = {} & a \frac{2^{1-2\alpha_k} \Gamma(2\alpha_k)}{\Gamma(\alpha_k)\Gamma(\alpha_k + 1)} \left(\frac{\lambda_k}{b\bar{\gamma}}\right)^{\alpha_k} \\ & \times {}_2F_1\left[\alpha_k, \frac{1}{2} + \alpha_k; 1 + \alpha_k; -\frac{\lambda_k}{b\bar{\gamma}}\right] \\ & - c\left[1 - \frac{4}{\pi} \sum_{n=0}^{\alpha_k - 1} \left(\frac{\lambda_k}{b\bar{\gamma}}\right)^n \frac{1}{(2n+1)} \right. \\ & \left. \times {}_2F_1\left(\frac{1}{2} + n, 1 + n; \frac{3}{2} + n; -1 - \frac{\lambda_k}{b\bar{\gamma}}\right)\right] \end{aligned} \tag{23}$$

where α_k and λ_k are the fading parameters of k-th hop and a, b and c are constants depending on the modulation scheme (for QPSK, $a = 1$, $b = 0.5$ and $c = 0.25$) [39].

Proof: See Appendix C. ■

1) SER ANALYSIS USING THE PDF OF e2e SNR

In addition to the upper bound of SER using per hop SERs, we also derive SER expressions based on PDF of e2e equivalent SNR (9), which provides an exact error expression if the error is assumed to occur in the link with worst SNR. This assumption simplifies SER derivations and essentially provides a tight lower SER bound, which converges to exact SER in high SNR region. Therefore, in the following three propositions, we provide the closed form expressions for equivalent SERs.

Proposition 6: For a class of noncoherent binary signaling, such as DBPSK and BFSK, equivalent e2e SER is given by

$$\begin{aligned} P_{\text{eq}} = {} & a \sum_{\mathbf{s}} p^{w(\mathbf{s})} q^{K - w(\mathbf{s})} \\ & \times \left(\Lambda_{\mathbf{s}} \sum_{m=0}^{\hat{k}} \frac{\mu_m^{\mathbf{s}} m!}{(b\bar{\gamma} + \Lambda_{\mathbf{s}})^{(m+1)}} - \sum_{m=1}^{\hat{k}} \frac{\mu_m^{\mathbf{s}} m!}{(b\bar{\gamma} + \Lambda_{\mathbf{s}})^m}\right), \end{aligned} \tag{24}$$

where a and b are constants depending on the modulation scheme (for DPSK, $a = 0.5$, and $b = 1$) [39].

Proof: In this case, SER can be written in the form $P_e(x) = a \exp(-bx)$. Now P_{eq} can be derived using (21) by replacing $f_{\gamma_k}(x)$ by $f_{\gamma_{\text{eq}}}(x)$ given in (9). Then the resulting expression can be simplified to (24) using [36, eq. 3.351.3] after some mathematical manipulations. ■

Proposition 7: For a class of coherent binary signaling, such as BPSK and BFSK, the equivalent e2e SER is given by

$$P_{\text{eq}} = a\sum_{\mathbf{s}} p^{w(\mathbf{s})} q^{K-w(\mathbf{s})}\Bigg(\Lambda_{\mathbf{s}}\sum_{m=0}^{\hat{k}}\frac{\mu_m^{\mathbf{s}}\Gamma\left(m+\frac{3}{2}\right)}{\sqrt{\pi}(m+1)(b\bar{\gamma})^{m+1}} \times {}_2F_1\left(1+m,\frac{3}{2}+m;2+m;-\frac{\Lambda_{\mathbf{s}}}{b\bar{\gamma}}\right) - \sum_{m=1}^{\hat{k}}\frac{\mu_m^{\mathbf{s}}\Gamma\left(m+\frac{1}{2}\right)}{\sqrt{\pi}(b\bar{\gamma})^m}\,{}_2F_1\left(m,\frac{1}{2}+m;1+m;-\frac{\Lambda_{\mathbf{s}}}{b\bar{\gamma}}\right)\Bigg), \tag{25}$$

where a and b are constants depending on the modulation scheme (for BPSK, $a = 0.5$, $b = 1$) [39].

Proof: In this case, conditional SER can be written in the form $P_e(x) = a\,\text{erfc}\left(\sqrt{bx}\right)$. Then (25) can be derived using (21) by replacing $f_{\gamma_k}(x)$ with $f_{\gamma_{\text{eq}}}(x)$. ∎

Proposition 8: In case of quadrature and multi-level signaling, such as QPSK, MSK, and Square-QAM modulations, SER is given by

$$P_{\text{eq}} = I_1 - I_2, \tag{26}$$

where the expression for I_1 is same as the P_{eq} derived in (25) with modified value of a and b depending upon the modulation scheme and I_2 is given by

$$I_2 = c\sum_{\mathbf{s}} p^{w(\mathbf{s})} q^{K-w(\mathbf{s})}\left(J_1 - J_2\right) \tag{27}$$

where J_1 and J_2 are given by

$$J_1 = \sum_{m=0}^{\hat{k}}\frac{m!\mu_m^{\mathbf{s}}}{\Lambda_{\mathbf{s}}^m}\Bigg(1-\frac{4}{\pi}\sum_{n=0}^{m}\frac{\Lambda_{\mathbf{s}}^n}{(2n+1)\,(b\,\bar{\gamma})^n} \times {}_2F_1\left[\frac{1}{2}+n,1+n;\frac{3}{2}+n;-1-\frac{\Lambda_{\mathbf{s}}}{b\bar{\gamma}}\right]\Bigg), \tag{28}$$

$$J_2 = \sum_{m=1}^{\hat{k}}\frac{m!\mu_m^{\mathbf{s}}}{\Lambda_{\mathbf{s}}^m}\Bigg(1-\frac{4}{\pi}\sum_{n=0}^{m-1}\frac{\Lambda_{\mathbf{s}}^n}{(2n+1)\,(b\,\bar{\gamma})^n} \times {}_2F_1\left[\frac{1}{2}+n,1+n;\frac{3}{2}+n;-1-\frac{\Lambda_{\mathbf{s}}}{b\bar{\gamma}}\right]\Bigg). \tag{29}$$

Proof: The proof follows similar to (23) with averaging done over the PDF in (9). ∎

Equation (26) therefore provides a generalized e2e SER expression for a wide range or modulation schemes such as QPSK, MSK, and Square-QAM, which are applicable in mmWave communication. The computation involves the Gauss hypergeometric function which can be easily evaluated via MATLAB.

IV. PERFORMANCE OF INTERFERENCE LIMITED LINKS

Up to now, we ignored the effect of co-channel interference and derived coverage, ergodic capacity and SER. This assumption is valid for mmWave relay deployments where interference signals attenuate significantly due to blockages and high path losses [4]. However, network densification has emerged as a performance enabler of 5G wireless networks. In particular, ultra-dense networks with dense and massively deployed base stations, relays and access points can provide high data rates, better coverage, seamless connectivity and improved energy efficiency [23], [35]. However, co-channel interference then becomes the fundamental limiting factor, which must be considered in performance analysis [41].

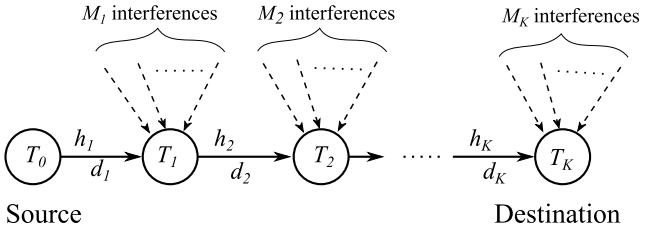

FIGURE 2. Co-channel interferences at relay and destination nodes.

Therefore, we next consider the interference-limited regime where the total interference is significantly higher than the additive noise. Thus we neglect the latter and focus on the statistical distribution of SIR. To this end, we analyze two distinct cases (i) when interference powers are i.i.d. r.v.s and (ii) when interference powers are i.n.i.d. r.v.s. Now, the received signal model in interference limited relaying is given by

$$y_{k,l} = \sqrt{Q_{k,l}}\,h_{k,l}\,x_{k-1} + \sum_{n=1}^{M_k}\sqrt{Q_{n,k}}\,h_{n,k}\,x_{n,k} \tag{30}$$

where $Q_{k,l}$, $h_{k,l}$ and x_{k-1} are same as in (2), M_k is the total number of co-channel interferers at T_k, $Q_{n,k}$ is the average received interference power at T_k from n-th interferer, $h_{n,k}$ is the normalized fading coefficient from n-th interferer to T_k which follows a Nakagami-m distribution, $x_{n,k}$ is the transmit symbol of each interferer which is assumed Gaussian with unit mean power [26]. A schematic diagram of a multi-hop network with multiple co-channel interferers at relays and destination is given in Fig. 2.

A. CASE 1: INTERFERENCE POWERS ARE I.I.D

In this case, k-th relay is subject to M_k number of interferers and the fading parameters of the received interference power $I_{n,k} = Q_{n,k}|h_{n,k}|^2$ are same for all n, $n \in \{1, 2, \cdots, M_k\}$. Thus, $I_{n,k}$ is distributed as $I_{n,k} \sim \mathcal{G}(\alpha_{I_k}, \lambda_{I_k}/\zeta_{I_k})$ where $\zeta_{I_k} = Q_{n,k}$ is the average interference power of n-th interferer at T_k which is assumed to be equal for all n. It is apparent that the total interference power $I_k = \sum_{n=1}^{M_k} I_{n,k}$ is distributed as $I_k \sim \mathcal{G}(M_k\alpha_{I_k}, \lambda_{I_k}/\zeta_{I_k})$. Assuming Nakagami-m fading of the desired signal, the received signal power S_k at T_k is distributed as $S_k \sim \mathcal{G}(\alpha_k, \lambda_k/\zeta_k)$, with $\zeta_k = Q_{k,l}$ being the average received signal power at T_k. Thus, the instantaneous SIR at T_k is the ratio of two independent Gamma r.v.s, i.e., $\xi_k = \frac{S_k}{I_k}$. It is well known that this ratio follows the beta prime distribution [42]. Thus, the PDF of ξ_k can be written as

$$f_{\xi_k}(x) = \frac{1}{\omega_k\bar{\xi}_k\,\mathcal{B}\,(\sigma_k,\theta_k)}\left(\frac{x}{\omega_k\bar{\xi}_k}\right)^{\sigma_k-1}\left(1+\frac{x}{\omega_k\bar{\xi}_k}\right)^{-\sigma_k-\theta_k}, \tag{31}$$

where $\sigma_k = \alpha_k$, $\theta_k = M_k\alpha_{I_k}$, $\omega_k = \frac{M_k\lambda_{I_k}}{\lambda_k}$, $\bar{\xi}_k = \frac{\zeta_k}{M_k\zeta_{I_k}}$ is the average SIR at T_k, and $\mathcal{B}(a,b) = \int_0^1 t^{a-1}(1-t)^{b-1}dt$ is the Euler's beta function. The CDF of ξ_k is given by

$$F_{\xi_k}(x) = \frac{1}{\sigma_k\,\mathcal{B}(\sigma_k,\theta_k)}\left(\frac{x}{\omega_k\bar{\xi}_k}\right)^{\sigma_k} \times {}_2F_1\left(\sigma_k, \sigma_k+\theta_k; 1+\sigma_k; -\frac{x}{\omega_k\bar{\xi}_k}\right). \quad (32)$$

Lemma 3: For a multi-hop DF network, with independent interference statistics at each relay, the SIR coverage probability is given by

$$P_{\text{cov}} = \sum_{\mathbf{s}} p^{w(\mathbf{s})}q^{K-w(\mathbf{s})}\prod_{k=1}^{K}\left[1 - \frac{1}{\sigma_k\,\mathcal{B}(\sigma_k,\theta_k)}\left(\frac{\gamma_{\text{th}}}{\omega_k\bar{\xi}_k}\right)^{\sigma_k} \times {}_2F_1\left(\sigma_k, \sigma_k+\theta_k; 1+\sigma_k; -\frac{\gamma_{\text{th}}}{\omega_k\bar{\xi}_k}\right)\right] \quad (33)$$

where summation across $\mathbf{s}$ *is to indicate that each hop can be in an LOS or NLOS state, similar to* (10).

Proof: Since $P_{\text{cov}} = \prod_{k=1}^{K}\tilde{F}_{\xi_k}(\gamma_{\text{th}})$, by using (32), this follows immediately. ∎

Moreover, if the distinct SIRs are identically distributed, P_{cov} has the convenient closed-form expression:

$$P_{\text{cov}} = 1 - \sum_{k=1}^{K}\binom{K}{k}(-1)^{k+1}\left[\frac{1}{\sigma\,\mathcal{B}(\sigma,\theta)}\left(\frac{\gamma_{\text{th}}}{\omega\bar{\xi}}\right)^{\sigma} \times {}_2F_1\left(\sigma, \sigma+\theta; 1+\sigma; -\frac{\gamma_{\text{th}}}{\omega\bar{\xi}}\right)\right]^{k} \quad (34)$$

where the subscript k and the summation across $\mathbf{s}$ are omitted since the SIR parameters at each relay are assumed identical and we only consider the state with all hops to be in LOS to study the performance in best link condition. This provides a convenient expression for the e2e coverage of multi-hop mmWave relay network by assuming SIRs have equal statistical distribution across all the hops. Although this case may not be practical, it provides insights on the effect of fading parameters of signal and interference on the coverage. Next, we present some results on coverage when interference powers are not identical across the relays.

B. CASE 2: INTERFERENCE POWERS ARE i.n.i.d.

In this case, we consider a total of M_k interferers at T_k with $M_{L,k}$ and $M_{N,k}$ respectively being the number of LOS and NLOS interferers, where $M_{L,k} + M_{N,k} = M_k$, $k \in \{1, \cdots, K\}$. Consider that the interference powers at node T_k are distributed with $I_{n,k} \sim \mathcal{G}(\alpha_{n,k}, \lambda_{n,k}/\zeta_{I_{n,k}})$ where $n \in \{1, 2, \cdots, M_k\}$, $\alpha_{n,k}$ and $\lambda_{n,k}$ are the channel fading parameters and $\zeta_{I_{n,k}}$ is the average interference power from n-th interferer to T_k. Similar to the i.i.d. case, we consider the desired signal power at T_k to be distributed as $S_k \sim \mathcal{G}(\alpha_k, \lambda_k/\zeta_k)$.

1) APPROXIMATE CDF OF PER HOP SIR

The distribution of total interference $I_k = \sum_{n=1}^{M_k} I_{n,k}$ is in general fairly complicated. Moreover, even if all $\alpha_{n,k}$'s are integers, the exact distribution, which can be derived, is very complicated and cumbersome. To avoid this problem, we may assume that I_k is approximately a Gamma r.v. The shape and rate parameters of this r.v. can be obtained by moment matching. This method is known as the *Welch-Satterthwaite Approximation* for the sum of gamma random variables [28], [29]. The approximation is summarized in the following lemma.

Lemma 4: Let $Y = X_1 + X_2 + \cdots + X_{M_k}$, *with mutually independent* $X_n \sim \mathcal{G}(\alpha_n, \lambda_n)$ *for* $n = 1, \ldots, M_k$. *Then* Y *is approximately* $\mathcal{G}(\alpha_y, \lambda_y)$, *where* $\alpha_y = \frac{\mu^2}{\sum_{n=1}^{M_k}\alpha_n\lambda_n^2}$, $\lambda_y = \frac{\mu}{\alpha_y}$ *and* $\mu = \sum_{n=1}^{M_k}\alpha_n\lambda_n$.

Accordingly, total interference I_k is approximately a $\mathcal{G}(\alpha_{I_k}, \lambda_{I_k})$ r.v., where $\alpha_{I_k} = \alpha_y$ and $\lambda_{I_k} = \lambda_y$ are obtained from Lemma 4. Now the PDF of k-th hop SIR is given by (31) with $\sigma_k = \alpha_k$, $\theta_k = \alpha_{I_k}$ and $\omega_k = \frac{\lambda_{I_k}}{\lambda_k}$, and the per-hop SIR CDF is given by (32). Now the e2e coverage probability can be computed using (33). Simulations show a very close match to this analytical result (Fig. 3), and consequently, the error due to the Welch-Satterthwaite approximation is negligible.

2) EXACT CDF OF PER HOP SIR

Although the exact expression of the PDF of e2e SIR is difficult to derive in a closed form, we can derive the exact CDF of per hop SIR for any number of interferers at a given relay by considering the signal power to be Gamma distributed with integer valued shape parameter. Then, the e2e SIR CDF can be written in terms of the product of individual hop SIR CDFs. To this end, in the following lemma, we provide the exact CCDF expression for k-th hop SIR.

Lemma 5: The exact expression for the CCDF of k*-th hop SIR for integer* α_k *is given by*

$$\tilde{F}_{\xi_k}(x) = \sum_{m=0}^{\alpha_k-1}\frac{(-1)^m(x\lambda_k/\zeta_k)^m}{m!}\mathcal{M}_{I_k}^m(x\lambda_k/\zeta_k), \quad (35)$$

where $\mathcal{M}_{I_k}^m(x\lambda_k/\zeta_k) = \frac{d^m\mathcal{M}_{I_k}(t)}{dt^m}|_{t=x\lambda_k/\zeta_k}$ *is the m-th moment of total interference power* I_k *at* T_k *computed at* $x\lambda_k/\zeta_k$, *and* $\mathcal{M}_{I_k}(t) = \prod_{n=1}^{M_k}\frac{\lambda_{n,k}^{\alpha_{n,k}}}{\left(\lambda_{n,k}+t\zeta_{I_{n,k}}\right)^{\alpha_{n,k}}}$ *is the moment generating function (MGF) of* I_k.

Proof: The proof is given in Appendix D. ∎

Now, using Lemma 5, the CCDF of e2e SIR is given by

$$\tilde{F}_{\xi_{\text{eq}}}(x) = \sum_{\mathbf{s}} p^{w(\mathbf{s})}q^{K-w(\mathbf{s})}\prod_{k=1}^{K}\left[1 - \sum_{m=0}^{\alpha_k-1}\frac{(-1)^m}{m!} \times (x\lambda_k/\zeta_k)^m\mathcal{M}_{I_k}^m(x\lambda_k/\zeta_k)\right]. \quad (36)$$

By substituting $x = \gamma_{\text{th}}$ in (36), exact e2e coverage probability can be readily obtained. However, using the CCDFs in (33) or (36) to evaluate other performance measures such as ergodic capacity and SER is difficult due to the product of K terms that complicates PDF expression of SIR.

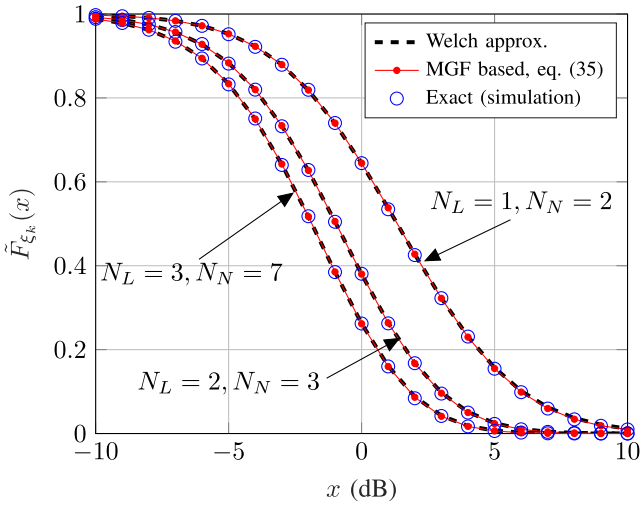

FIGURE 3. CCDF of per hop SIR plotted along x (dB) using *Welch-Satterthwaite Approximation* (Lemma 4), MGF approach (Lemma 5), and simulation. N_L and N_N denote the number of LOS and NLOS interferers, respectively, which are located at different distance to realize i.n.i.d.interference powers. The CCDF curves also refer to the per hop coverage probability along the SIR threshold of x dB.

C. ERGODIC CAPACITY

When evaluating the exact ergodic capacity of the multi-hop network, we make two simplifying assumptions.

1) Interference powers and SIRs at all the relays are i.i.d.. The more general i.n.i.d. case requires a very complicated expansion of (33), and thus is left as future work.
2) All the links are in LOS state. Since the SIRs at all relays are assumed i.i.d., the link states need to be identical, i.e., either all LOS or all NLOS. Although NLOS links are viable in mmWave network, the best case would be to have all LOS links. Note that, if the nodes are placed carefully, this condition is achievable. It also obviates the use of summation over $\mathbf{s}$ in the rest of the analysis.

Lemma 6: The CDF of the e2e SIR when per hop SIR are i.i.d. is given by

$$F_{\xi_{\text{eq}}}(x) = \sum_{k=1}^{K} \binom{K}{k} \frac{(-1)^{k+1}}{(\sigma\, \mathcal{B}(\sigma,\theta))^k} \sum_{m=0}^{n^\dagger} \kappa_m \left(\frac{x}{x+\omega\bar{\xi}}\right)^{m+\sigma k} \quad (37)$$

where $n^\dagger = k(\theta-1)$ and κ_m is the coefficient which can be computed recursively.

Proof: See Appendix E. ∎

Lemma 7: The PDF of e2e SIR can be written as

$$f_{\xi_{\text{eq}}}(x) = \sum_{k=1}^{K} \binom{K}{k} \frac{(-1)^{k+1}}{(\sigma\, \mathcal{B}(\sigma,\theta))^k} \sum_{m=0}^{n^\dagger} (m+\sigma k)\kappa_m \times \frac{\omega\bar{\xi}}{(x+\omega\bar{\xi})^2} \left(\frac{x}{x+\omega\bar{\xi}}\right)^{(m+\sigma k-1)}. \quad (38)$$

Proof: We arrive at (38) by differentiating $F_{\xi_{\text{eq}}}(x)$ in (37). ∎

Having the CDF and PDF of e2e SIR, we proceed to derive ergodic and asymptotic capacities below.

1) EXACT ERGODIC CAPACITY

Proposition 9: The ergodic capacity of interference limited multi-hop network is given by

$$\tilde{C} = \frac{1}{2\ln 2} \sum_{k=1}^{K} \binom{K}{k} \frac{(-1)^{k+1}}{(\sigma\, \mathcal{B}(\sigma,\theta))^k} \sum_{m=0}^{n^\dagger} (n+1)\kappa_m \times \left\{ \left[\frac{\sum_{j=1}^{n} \frac{1}{j} + \ln\left(\omega\bar{\xi}\right)}{n+1} \right] + \frac{(-1)^n}{n+1} \frac{\ln\left(\omega\bar{\xi}\right)}{\left(\omega\bar{\xi}-1\right)^{n+1}} + \sum_{k=1}^{n} (-1)^{k+1} \frac{\Gamma(k+1)\Gamma(n+1-k)}{k\left(\omega\bar{\xi}\right)^k \Gamma(n+2)} + \frac{(-1)^{n+1}}{n+1} \sum_{l=1}^{n} \frac{\left(\omega\bar{\xi}-1\right)^{-l}}{l\left(\omega\bar{\xi}\right)^{n+1-l}} \sum_{j=0}^{n-l} (-1)^j \binom{n-l}{j} \times \frac{l}{(l+j)\left(1-\omega\bar{\xi}\right)^j} \right\}, \quad (39)$$

where $n = m + \sigma k - 1$.

Proof: See Appendix F. ∎

Equation (39) provides the exact ergodic capacity as a function of average per hop SIR $\bar{\xi}$ for interference limited relays. Note that, as the number of hops increases, average per hop SIR also increases due to shorter links.

2) ASYMPTOTIC CAPACITY

To get direct insights on the capacity, we provide Proposition 10.

Proposition 10: As $\bar{\xi} \to \infty$, the asymptotic capacity of the multi-hop network is given by

$$\tilde{C}_{\text{high SIR}} = \frac{1}{2\ln 2} \left[\ln(\omega\bar{\xi}) + \sum_{k=1}^{K} \binom{K}{k} \frac{(-1)^{k+1}}{(\sigma\, \mathcal{B}(\sigma,\theta))^k} \times \sum_{m=0}^{n^\dagger} \kappa_m \left(\sum_{j=1}^{m+\sigma k-1} \frac{1}{j} \right) \right]. \quad (40)$$

Proof: The proof follows similar to (14) and is omitted here. ∎

When compared to (39), (40) includes only the first summation term in (39) and provides a simplified capacity expression giving insights on SIR dependence of capacity in asymptotic region; clearly, the capacity has a dominant term of $\ln(\bar{\xi})$, which shows a logarithmic growth over the average SIR.

D. SER ANALYSIS

To evaluate the SER in interference limited regime, we follow the similar technique as in noise limited analysis of Section III-E and use (19) to evaluate the SER at the receiver with new expressions for per hop SIR PDFs which are specified in the following propositions.

1) SER OF NONCOHERENT BINARY SIGNALING

Proposition 11: For a class of noncoherent binary signaling, such as DBPSK and FSK, k-th hop SER is given by

$$P_k = \frac{a}{\mathcal{B}(\sigma_k, \theta_k)} \sum_{j=0}^{\theta_k - 1} (-1)^j \binom{\theta_k - 1}{j} \Gamma(\sigma_k + j) \times U\left(\sigma_k + j, 0, b\omega_k \bar{\xi}_k\right) \quad (41)$$

where $U(\cdot)$ is a confluent hypergeometric function of the second kind [36, eq. 9.211.4].

Proof: The proof follows similar to (20) by replacing $f_{\gamma_k}(x)$ with $f_{\xi_k}(x)$. ∎

Proposition 12: For a class of noncoherent binary signaling, such as DBPSK and FSK, equivalent e2e SER is given by

$$P_{\text{eq}} = a \sum_{k=1}^{K} \binom{K}{k} \frac{(-1)^{k+1}}{(\sigma\, \mathcal{B}(\sigma, \theta))^k} \sum_{m=0}^{n^\dagger} \kappa_m (m + \sigma k)! \times U\left(m + \sigma k, 0, b\omega \bar{\xi}\right). \quad (42)$$

Proof: The proof follows similar to (20) by replacing $f_{\gamma_k}(x)$ with $f_{\xi_{\text{eq}}}(x)$. ∎

2) SER OF COHERENT BINARY SIGNALING

Proposition 13: For a class of coherent binary signaling, such as PSK and FSK, k-th hop SER is given by

$$P_k = \frac{a}{\mathcal{B}(\sigma_k, \theta_k)} \sum_{j=0}^{\theta_k - 1} \frac{(-1)^j}{\sqrt{\pi}(\sigma_k + j)} \binom{\theta_k - 1}{j} \times \Gamma\left(\sigma_k + j + \frac{1}{2}\right) U\left(\sigma_k + j, \frac{1}{2}, b\omega_k \bar{\xi}_k\right). \quad (43)$$

Proof: The proof follows similar to (22) by replacing $f_{\gamma_k}(x)$ with $f_{\xi_k}(x)$. ∎

Proposition 14: For a class of coherent binary signaling, such as PSK and FSK, equivalent e2e SER is given by

$$P_{\text{eq}} = a \sum_{k=1}^{K} \binom{K}{k} \frac{(-1)^{k+1}}{(\sigma\, \mathcal{B}(\sigma, \theta))^k} \sum_{m=0}^{n^\dagger} \frac{\kappa_m}{\sqrt{\pi}} \times \Gamma\left(m + \sigma k + \frac{1}{2}\right) U\left(m + \sigma k, \frac{1}{2}, b\omega \bar{\xi}\right) \quad (44)$$

Proof: The proof follows similar to (22) by replacing $f_{\gamma_k}(x)$ with $f_{\xi_{\text{eq}}}(x)$. ∎

Note that, SER expressions (41) through (44) provide the SER for binary modulations such as DBPSK and BPSK. Due the space limit, we do not analyze the SER of MPSK, M-QAM and other modulations. For this purpose, classical MGF techniques may also be useful [43], [44]. Thus, further analysis is left as potential future work.

V. RESULTS AND DISCUSSION

Here, we verify our analytical results by comparing with Monte-Carlo simulations. Each simulation run has 10^5 independent channel realizations. Table 1 lists our simulation parameters. In all figures, curves and markers represent the analytical results and simulation results, respectively. In all cases, the analytical and simulation results show a perfect match, verifying the correctness of the analytical derivations. We discuss the results separately for noise-limited and interference-limited regimes.

TABLE 1. Notations and simulation parameters.

Notation	Parameter	Value
P_T	Total transmit power	30 dBm
D	Total source to destination distance	500 m
f	Operating frequency	28 GHz
W	System bandwidth	100 MHz
ν_L, ν_N	LOS and NLOS path loss exponents	2, 3.3
m_L, m_N	Nakagami-m parameters for LOS and NLOS cases	3, 2 [27]
$G_{\max}, G_{\min}$	Main lobe and side lobe gains	18 dBi, -2 dBi
ϕ	half power beamwidth	30°
η	Blockage density	$5 \times 10^{-4} (1/m^2)$
$\mathbb{E}[L], \mathbb{E}[W]$	Average blockage length, width	15 m, 15 m
N_0	Noise power	-174 dBm/Hz + $10\log_{10}(W) + 10$ dB

A. NOISE-LIMITED REGIME

In Fig. 4, we plot coverage probability (10) as a function of the threshold, parameterized by the number of hops to cover the total distance $D = 500$ meters for the noise-limited scenario. The total distance is divided equally among K hops and for the fairness in comparison, we use a constant total transmit power P_T and use $\mathcal{P}_k = P_T/K$ for $k = 0, \cdots, K-1$. It is evident that the coverage improves with increasing hops K, which is evident by the right shift in the curves with K. For example, at $\gamma_{\text{th}} = 5$ dB, SNR coverage improves from 40% to 96% when going from $K = 2$ to $K = 5$. However, the improvement in coverage probability diminishes with increasing K.

Fig. 5 plots the outage probability versus average per hop SNR for different number of hops and different SNR thresholds for noise-limited case. Outage probability is evaluated using $1 - P_{\text{cov}}$ where P_{cov} is from (10) and is computed for a given value of average SNR and SNR threshold. This figure clearly shows that the outage probability increases significantly with the increase in SNR thresholds. However, the outage increases slightly with the increasing number of hops from 2 to 5. Note that, here the outage probability comparison is performed along average per hop SNR and, as a result, the increase in the number of hops appears to increase the outage probability due to the cumulative effect of outage events in each hop. However, in practice, when the number of hops is increased, average per hop SNR increases which corresponds to the decrease in outage probability (or increase in coverage probability) which is already discussed in Fig 4.

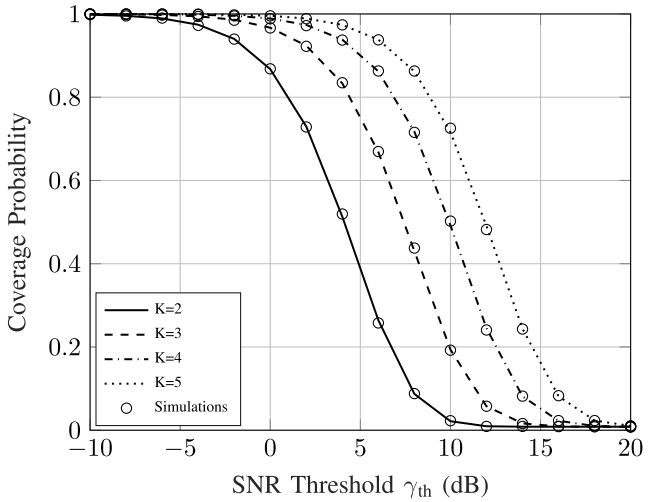

FIGURE 4. Coverage versus SNR thresholds for different K.

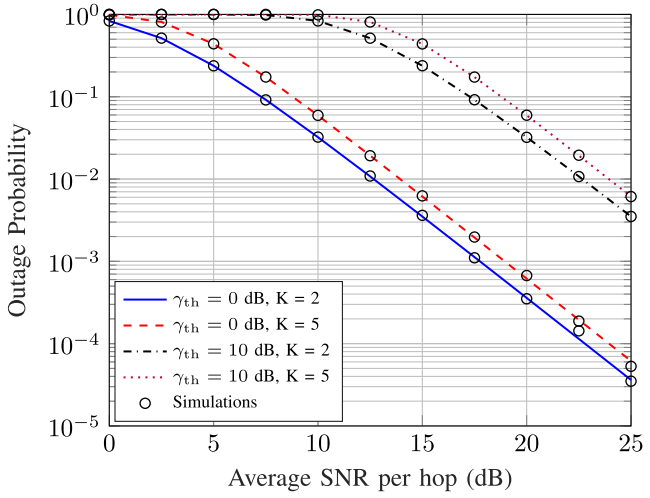

FIGURE 5. Outage Probability versus average per hop SNR for different SNR thresholds.

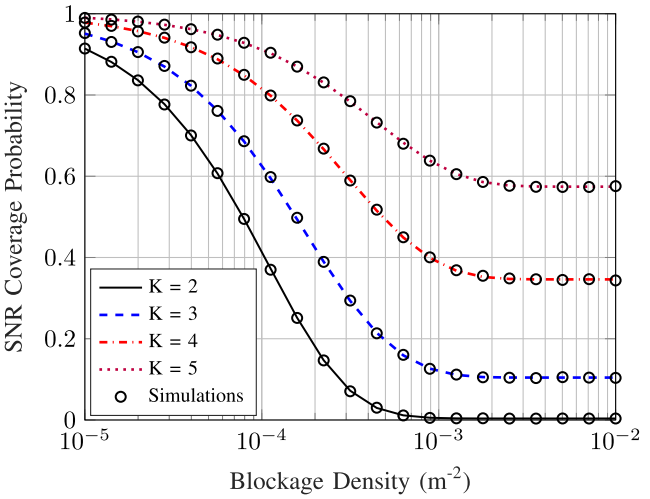

FIGURE 6. Coverage probability versus blockage density (η) at γ_{th} = 10 dB for different number of hops (K), D = 500 m.

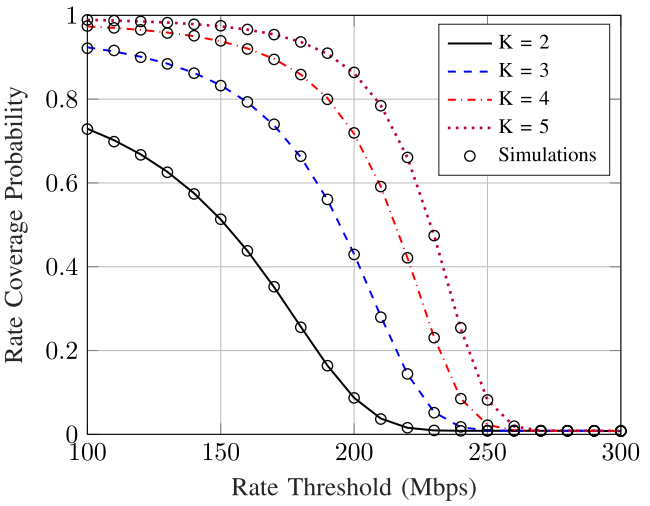

FIGURE 7. Rate coverage versus rate threshold (D = 500) m.

Fig. 6 plots coverage probability (10) as a function of blockage density η for an SNR threshold of 10 dB. Note, in (10), we have $p = e^{-\beta d}$ and $q = 1 - p$ with β being a function of η (Sec. II-D) and $d = D/K$. The expected length and width of blockage objects are assumed to be 15 meters for urban and semi-urban areas. Typical building dimensions are close to these values [34]. The increasing number of hops clearly improves coverage for entire range of blockage density. For example, for a blockage environment with density 10^{-4} (100 blockage objects/km^2),[2] coverage improves from 40% to 90% from two hops to five hops. This remarkable improvement illustrates the effectiveness of multi-hop links to overcome mmWave blockages. However, coverage probability flattens when the blockage density exceeds a threshold. The reason is that when there are too many blocking objects, all the links are likely to be NLOS. The flattening point shifts right with the increased number of hops since the link distance decreases with increasing K and LOS probability is higher for a shorter link. Practically, 10^{-2} is a very high density (10,000 blockage objects/km^2) and is shown here just to study the coverage in a very high density blockage environment.

To evaluate the data rate achievable with the number of hops, we plot the rate coverage probability (12) versus rate threshold for different number of hops in Fig. 7. As these plots show, the rate coverage increases with more hops. This is because of the decreased per hop distance resulting in higher SNR. For example, 200 Mbps coverage improves from about 10% to about 87% when increasing K from 2 to 5. However, the coverage gain diminishes as K keeps increasing, which suggests that a careful choice of the number of hops must be based on the required rate coverage.

[2]This blockage density is practical for a typical urban scenario.

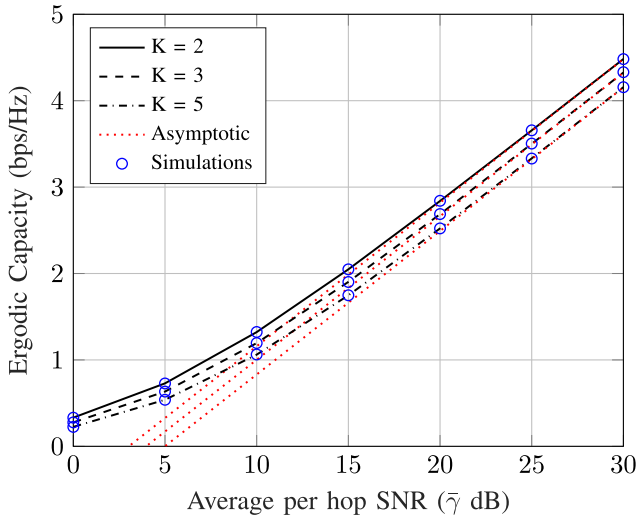

FIGURE 8. Ergodic capacity versus $\bar{\gamma}$, $K = 2, 3, 5$.

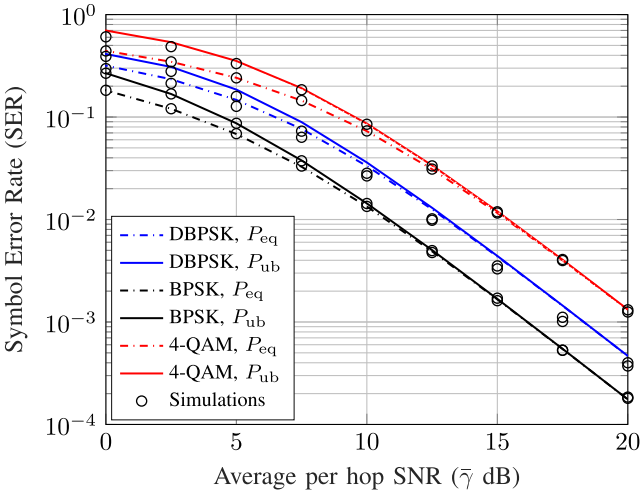

FIGURE 9. SER versus $\bar{\gamma}$ for DBPSK, BPSK and 4-QAM, K = 3.

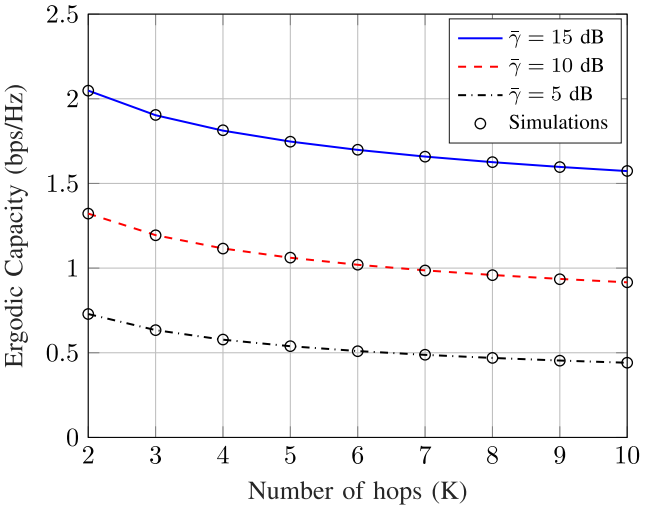

FIGURE 10. Ergodic capacity versus number of hops (K) for different average per hop SNRs.

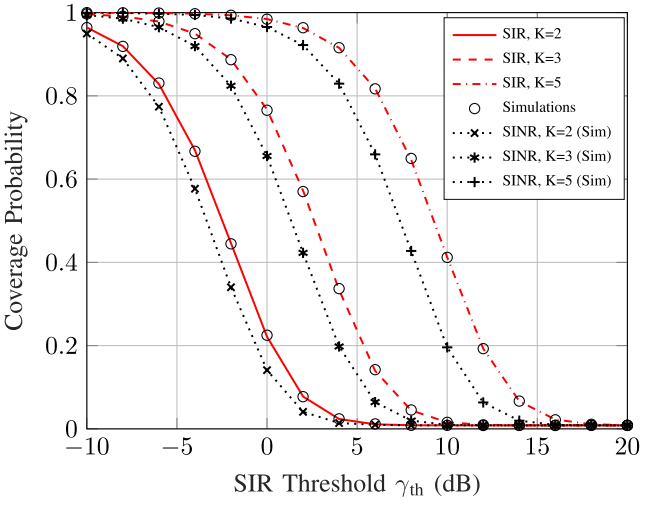

FIGURE 11. Coverage versus SIR thresholds for different K.

In Fig. 8, we plot the ergodic capacity (bps/Hz).[3] of the noise limited multi-hop relay link versus the average per hop SNR (13). We assume that co-channel relay transmission is avoided only between immediate neighbors and alternately located relays can transmit in the same time slot. The plots show that, for a fixed $\bar{\gamma}$, ergodic capacity slightly decreases when the number of hops increases. As expected, the asymptotic capacity lines in (14) appear to converge to exact capacity for higher SNR values.

The effect of multi-hop transmission on the SERs of DBPSK, BPSK and 4-QAM versus average per hop SNR in Section III-E is plotted in Fig. 9 for $K = 3$. We have plotted P_{ub} and P_{eq} to compare the two classes of SER expressions which consider the error occurring in any link or error occurring in the weakest SNR link. The effect of increasing hops (not shown in the figures) shows that SER increases slightly with increasing $K = 3$ to $K = 5$ when SNR per hop is fixed. However, increasing the hops increases the average SNR per hop due to the decreased distance and higher LOS probability per hop, which can compensate for the increased SER due to multiple hops.

Fig. 10 plots the effect of total number of hops on ergodic capacity of the multi-hop network (13) for different average SNRs. Clearly, the capacity is higher for higher value of $\bar{\gamma}$ and it decreases with increase in K for given $\bar{\gamma}$. However, the capacity curves do not fall sharply because we assume that the multiplexing gain is fixed at $1/2$ and is independent of K. This signifies the suitability of multi-hop relays in mmWave networks.

B. INTERFERENCE-LIMITED REGIME

In Fig. 11, we plot coverage probability (33) for a varying number of hops to cover the total distance $D = 500$ meters for interference-limited scenario. Similar to

[3]Here, the achievable user rate is determined by the bandwidth assigned to the user. For example, if a bandwidth of 1 GHz is used, rates of above 1 Gbps are achieved for $\bar{\gamma} = 10$ dB, which exceed the user perceived data rate of 100 Mbps specified for 5G in IMT-2020 requirement [45]

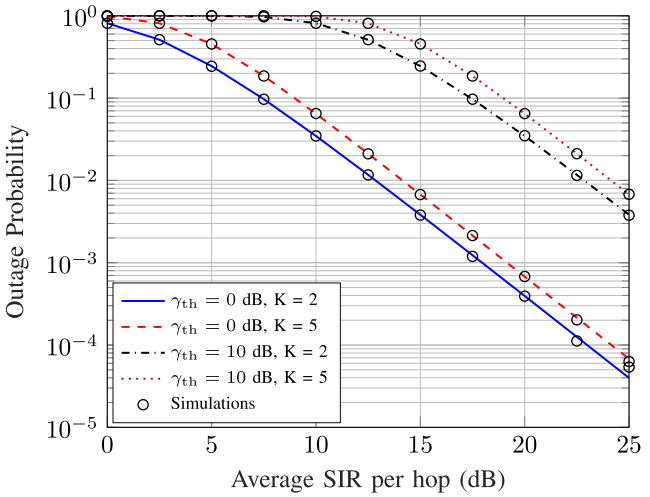

FIGURE 12. Outage probability versus average per hop SIR for different SIR thresholds.

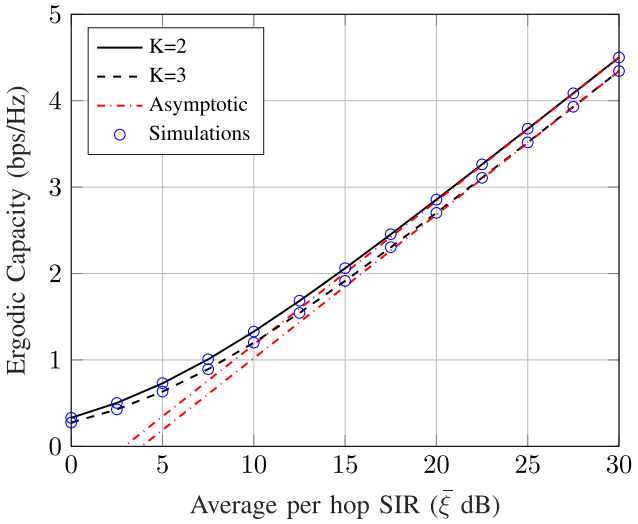

FIGURE 13. Ergodic capacity versus $\bar{\xi}$, K = 2, 3.

existing works [12], [15] dealing with interference-limited multi-hop links, we consider a fixed number of interferers at each relay and the destination independent of the number of hops.[4] Specifically, 5 NLOS interferers located at a distance of 100 meters from each node are assumed. The coverage improves with increasing K, which is evident by the right shift in the SIR curves with K. For example, at $\gamma_{\text{th}} = 5$ dB, SIR coverage increases from 2% to 88% from two hops to five hops. This trend is due to the smaller path loss in shorter links. We also simulate coverage probability considering both noise and interference (labeled SINR). As expected, the coverage is lower in this case compared to when only interference is considered. But the SINR coverage also improves with increase in the number of hops. The gap between the SIR and SINR curves increases with K because of the following reason. When the number of hops increases, the distance of each hop decreases, which means a larger received power level of desired signal at the receiver of the hop. Since each relay is impaired by a fixed number of interferers, increasing K does not affect much the interference level over a hop. Thus, when K increases, the gap between SIR and SINR for a hop becomes larger. As a result, the gap between the end-to-end SIR and end-to-end SINR also increases.

Fig. 12 plots the outage probability versus average per hop SIR for different number of hops and different SIR thresholds. Outage probability is evaluated using $1 - P_{\text{cov}}$ where P_{cov} is in (33) and is computed for a given value of average SIR and SIR threshold. We observe that, outage probability curves are almost identical to those for noise-limited scenario. In addition, it is clearly seen that the outage probability increases significantly with the increase in SIR thresholds. However, the outage probability increases slightly with the increasing number of hops from 2 to 5.

[4]This setting is reasonable due to the following reason. Consider the density of interferers is fixed, and thus, each node (a relay or the destination in our multiple-hop link) expects to receive a similar amount of interference. Thus, we consider a given number of interferers at each relay and the destination in our system.

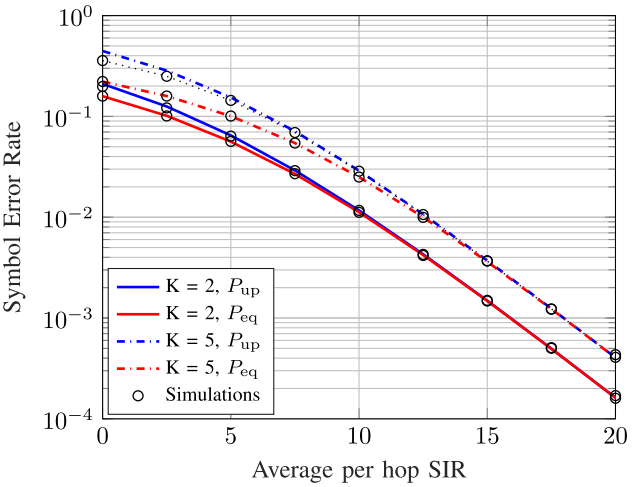

FIGURE 14. SER versus $\bar{\xi}$ for BPSK for K = 2 and K = 5.

In Fig. 13 we plot the ergodic capacity (39) of the interference-limited network along average SIR per hop. Similar to noise limited scenario, the capacity decreases by increasing the number of hops when plotted against the average per hop SIR. For example, at $\bar{\xi} = 10$ dB, it decreases from 1.3 bps/Hz to 1.2 bps/Hz when increasing the number of hops from 2 to 3. However, when K increases, the average SIR increases resulting the capacity to improve.

To study the SER in interference limited scenario, Fig. 14 plots the SER versus SIR of BPSK from Section IV-D.2 for $K = 2$ and $K = 5$. SER increases along with the increase in number of hops similar to that of the noise limited case. Likewise, P_{eq} converges to P_{up} for higher SIR values.

VI. CONCLUSION

In this paper, we have analyzed the coverage, capacity and symbol error rates of the mmWave multi-hop link in noise-limited and interference-limited scenarios. For the

noise-limited scenario, we first derived the distribution of equivalent e2e SNR considering the LOS and NLOS conditions of the individual links. We also derived the closed-form expressions for coverage probability, rate coverage, ergodic capacity, and symbol error rates for DBPSK, BPSK and Square-QAM modulations. For interference-limited scenario, we first derived per-hop SIR distribution considering i.i.d. and i.n.i.d. interference powers. Then, we derived the e2e capacity and SER for DBPSK and BPSK modulations. Based on our analysis and numerical results, following observations can be made:

- Coverage probability improves significantly when multiple hops are used. However, if the per hop SNR is fixed, outage probability and SER get increased due to cumulative effect of outage events in each hop when the number of hops increases.
- The effect of the density of blocking objects in coverage probability is significant; however, it can be compensated by increasing the number of hops.
- The noise-limited and interference-limited scenarios show similar trend of ergodic capacity (decreasing with increasing number of hops) and symbol error rates (increasing with increasing number of hops) for a given SNR/SIR. However, actual received SNR/SIR is found to increase (Fig. 4, Fig. 11) due to shorter link lengths which compensate for decreased performance caused by increased number of hops.

In this paper, we focus on performance of a multi-hop mmWave link. Recently, IEEE 802.11ad standard suggests dual-band communications [46]. In specific, the fast session transfer (FST) adopted in IEEE 802.11ad standard defines an inter-operation policy between 2.4/5 GHz and 60 GHz wireless channels. If the FST-based dual-connectivity technique is applied to our system, the coverage and rate performance can be further improved. For example, if a multi-hop link operates in dual bands, it can be switched from mmWave to sub-6 GHz band when achieved SNR or SIR in mmWave band falls below a required threshold. In this case, the coverage in mmWave band remains the same as derived in our paper. Our analysis in our paper can also be used to derive the coverage of the sub-6 GHz band due to the following reason. For sub-6 GHz channel, Rayleigh fading model is commonly used in the literature which results in exponentially distributed signal and co-channel interference powers. This can be easily adapted in our analysis because we are using Gamma distributed signal and interference powers which convert to exponential distribution when shape parameter of Gamma random variable is set to 1. Denote P_{cov1} as the coverage probability in mmWave band and P_{cov2} as the coverage probability in the sub-6 GHz band. Then the overall coverage probability of the dual-band system is given by $P_{\text{cov}} = 1 - (1 - P_{\text{cov1}})(1 - P_{\text{cov2}})$, which is larger than both P_{cov1} and P_{cov2}. Therefore, including dual bands will further improve the coverage presented in our paper. In a similar way, rate performance can also be improved.

For future work, interference analysis considering the spatial locations of the relays and interferers using the tools from stochastic geometry can be developed. Moreover, our work can be extended to study the SER performance of multi-hop relaying for other modulation schemes.

APPENDIX A: PROOF OF LEMMA 2

Proof: Since $\tilde{F}_{X_{\min}}(x) = \prod_k \tilde{F}_{X_k}(x)$, $\alpha_k \in \mathbb{N}$, and $\tilde{F}_{X_k}(x) = e^{-\lambda_k x} \sum_{n=0}^{\alpha_k - 1} \frac{(\lambda_k x)^n}{n!}$, we find CCDF of equivalent e2e SNR as

$$\tilde{F}_{\gamma_{\text{eq}}}(x) = e^{-(\lambda_1 + \cdots + \lambda_K)x} \underbrace{\prod_{k=1}^{K} \sum_{n=0}^{\alpha_k - 1} \frac{(\lambda_k x)^n}{n!}}_{P}, \quad 0 \le x < \infty, \tag{45}$$

where the product term P can be expanded as

$$P = \sum_{n_1=0}^{\alpha_1 - 1} a_{1_n} x^{n_1} \cdot \sum_{n_2=0}^{\alpha_2 - 1} a_{2_n} x^{n_2} \cdots \sum_{n_K=0}^{\alpha_K - 1} a_{K_n} x^{n_K} \tag{46}$$

where $a_{k_n} = \frac{\lambda_k^{n_k}}{n_k!}$, $k = 1, 2, \cdots, K$. The above expression is the product of K number of $(\alpha_k - 1)$-th degree polynomials which can be readily computed using the convolution of coefficients. Clearly, P is a polynomial in x of degree $\sum \alpha_k - K$. By symbolically multiplying the K polynomials of P and collecting all the terms corresponding to the coefficient of x^m, we get Lemma 2. ■

APPENDIX B: PROOF OF THEOREM 3

Proof: Since we have the CDF expression of the e2e SNR, we can compute ergodic capacity as

$$\begin{aligned} \tilde{C} &= \frac{1}{2\ln 2} \int_0^\infty \ln(1+x) f_{\gamma_{\text{eq}}}(x) dx \\ &= -\frac{1}{2\ln 2} \int_0^\infty \ln(1+x) d\tilde{F}_{\gamma_{\text{eq}}}(x) \\ &= \frac{1}{2\ln 2} \int_0^\infty \frac{\tilde{F}_{\gamma_{\text{eq}}}(x)}{(1+x)} dx \end{aligned} \tag{47}$$

where $\tilde{F}_{\gamma_{\text{eq}}}(x)$ is the CCDF of equivalent e2e SNR given in (8). Now, solving the integral in (47), we obtain (13). ■

APPENDIX C: PROOF OF PROPOSITION 5

For QPSK, MSK, and Square-QAM modulations, conditional SER can be written in the form $P_k(x) = a\,\text{erfc}\left(\sqrt{bx}\right) - c\,\text{erfc}^2\left(\sqrt{bx}\right)$. Now P_k is given by averaging over k-th hop SNR PDF as

$$\begin{aligned} P_k &= \int_0^\infty \left(a\,\text{erfc}\left(\sqrt{bx}\right) - c\,\text{erfc}^2\left(\sqrt{bx}\right)\right) f_{\gamma_k}(x) dx \\ &= I_1 - I_2 \end{aligned} \tag{48}$$

where $f_{\gamma_k}(x)$ is same as in (21), and the first integral I_1 is same as (22) in Proposition 4 with a and b depending on modulation

scheme. The second integral I_2 is given by

$$I_2 = \frac{c}{\Gamma(\alpha_k)}\left(\frac{\lambda_k}{\bar{\gamma}}\right)^{\alpha_k}\int_0^{\infty} x^{m-1}\mathrm{e}^{-\frac{\lambda_k}{\bar{\gamma}}x}\mathrm{erfc}^2\left(\sqrt{bx}\right)dx. \tag{49}$$

Now with the help of [47, eq.(28)] and after some mathematical manipulations, we get

$$I_2 = c\Bigg[1 - \frac{4}{\pi}\sum_{n=0}^{\alpha_k-1}\left(\frac{\lambda_k}{b\bar{\gamma}}\right)^n \frac{1}{(2n+1)} \times {}_2F_1\left(\frac{1}{2}+n, 1+n; \frac{3}{2}+n; -1-\frac{\lambda_k}{b\bar{\gamma}}\right)\Bigg]. \tag{50}$$

Finally substituting I_1 and I_2, we obtain (23).

APPENDIX D: PROOF OF LEMMA 5

Consider $S_k \sim \mathcal{G}(\alpha_k, \lambda_k/\zeta_k)$ be the desired signal power and the interference powers are distributed with $I_{n,k} \sim \mathcal{G}(\alpha_{n,k}, \lambda_{n,k}/\zeta_{I_{n,k}})$ where $n \in \{1, 2, \cdots, M_k\}$ with total of M_k interferers at T_k. Now the CCDF of ξ_k is given by

$$\begin{aligned}\tilde{F}_{\xi_k}(x) &= \mathbb{P}\left(\xi_k > x\right) = \mathbb{P}\left(\frac{S_k}{I_k} > x\right)\\ &= \mathbb{P}\left(S_k > xI_k\right) = \mathbb{E}_{I_k}\left[\frac{\Gamma\left(\alpha_k, x\, I_k\lambda_k/\zeta_k\right)}{\Gamma\left(\alpha_k\right)}\right]\\ &= \mathbb{E}_{I_k}\left[\mathrm{e}^{-xI_k\lambda_k/\zeta_k}\sum_{m=0}^{\alpha_k-1}\frac{(xI_k\lambda_k/\zeta_k)^m}{m!}\right]\\ &= \sum_{m=0}^{\alpha_k-1}\frac{1}{m!}\mathbb{E}_{I_k}\left[(xI_k\lambda_k/\zeta_k)^m\,\mathrm{e}^{-(xI_k\lambda_k/\zeta_k)}\right]\\ &= \sum_{m=0}^{\alpha_k-1}\frac{(-1)^m(x\lambda_k/\zeta_k)^m}{m!}\mathcal{M}_{I_k}^m\left(x\lambda_k/\zeta_k\right)\end{aligned} \tag{51}$$

where $I_k = \sum_{n=1}^{M_k} I_{n,k}$ is the total interference power at T_k and the m-th moment of I_k, $\mathcal{M}_{I_k}^m(t)$ can be obtained using the MGF of I_k which is given by

$$\begin{aligned}\mathcal{M}_{I_k}(t) &= \mathbb{E}\left[\mathrm{e}^{-tI_k}\right] = \mathbb{E}\left[\mathrm{e}^{-t\sum_{n=1}^{M_k} I_{n,k}}\right]\\ &= \prod_{n=1}^{M_k}\frac{\lambda_{n,k}^{\alpha_{n,k}}}{\left(\lambda_{n,k}+t\zeta_{I_{n,k}}\right)^{\alpha_{n,k}}},\end{aligned} \tag{52}$$

where the product in last equality is using the property of MGF of sum of independent gamma random variables.

APPENDIX E: PROOF OF LEMMA 6

Using (34) for identical per hop SIRs, the CDF of e2e SIR can be written as

$$F_{\xi_{\mathrm{eq}}}(x) = \sum_{k=1}^{K}\binom{K}{k}(-1)^{k+1}\Bigg[\frac{1}{\sigma\,\mathcal{B}(\sigma,\theta)}\left(\frac{x}{\omega\bar{\xi}}\right)^{\sigma} \times {}_2F_1\left(\sigma, \sigma+\theta, 1+\sigma, -\frac{x}{\omega\bar{\xi}}\right)\Bigg]^k. \tag{53}$$

Now, using the transformation formula for hypergeometric function [36, eq. 9.131.1], (53) can be rewritten as

$$F_{\xi_{\mathrm{eq}}}(x) = \sum_{k=1}^{K}\binom{K}{k}\frac{(-1)^{k+1}}{(\sigma\,\mathcal{B}(\sigma,\theta))^k}\left(\frac{x}{x+\omega\bar{\xi}}\right)^{\sigma k} \times\Bigg[{}_2F_1\left(\sigma, -(\theta-1); 1+\sigma; \frac{x}{x+\omega\bar{\xi}}\right)\Bigg]^k. \tag{54}$$

Now, because its second argument is a negative integer, the hypergeometric function in (54) truncates after the θ-th term. Thus, it can be conveniently written as a finite series as follows:

$${}_2F_1\left(\sigma, -(\theta-1); 1+\sigma; \frac{x}{x+\omega\bar{\xi}}\right) = \sum_{j=0}^{\theta-1}\delta_j\left(\frac{x}{x+\omega\bar{\xi}}\right)^j \tag{55}$$

where δ_j is given by

$$\delta_j = (-1)^j\binom{\theta-1}{j}\left(\frac{\sigma}{\sigma+j}\right).$$

Now substituting (55) in (54), we need to compute the k-th power of the sum in (55). Note that this product results in a polynomial of degree $k(\theta-1)$, where the polynomial coefficients can be computed as a convolution sum of the individual coefficients. With this, the polynomial representation becomes

$$\left[\sum_{j=0}^{\theta-1}\delta_j\left(\frac{x}{x+\omega\bar{\xi}}\right)^j\right]^k = \sum_{m=0}^{n^{\dagger}}\kappa_m\left(\frac{x}{x+\omega\bar{\xi}}\right)^m \tag{56}$$

where $n^{\dagger} = k(\theta-1)$ and κ_m are the polynomial coefficients computed using convolution. Now substituting (56) into (54), we obtain (37).

APPENDIX F: PROOF OF PROPOSITION 9

Proof: By averaging the instantaneous capacity over the e2e SIR PDF in (38), ergodic capacity can be written as

$$\tilde{C} = \frac{1}{K\ln 2}\sum_{k=1}^{K}\binom{K}{k}\frac{(-1)^{k+1}}{(\sigma\,\mathcal{B}(\sigma,\theta))^k}\sum_{m=0}^{n^{\dagger}}(n+1)\kappa_m I_n(a) \tag{57}$$

where $n = m+\sigma k-1$, $a = \omega\bar{\xi}$, and $I_n(a)$ is given by

$$I_n(a) = \int_0^{\infty}\ln\,(1+ax)\frac{x^n}{(x+1)^{n+2}}dx \tag{58}$$

where $a > 1$. To develop closed-form $I_n(a)$, we transform (58) as a Mellin integral [48]

$$I_n(a) = \frac{1}{2\pi j}\int_{c-j\infty}^{c+j\infty}\underbrace{\frac{\Gamma(s)\Gamma(1+s)\Gamma(1-s)\Gamma(n+1-s)}{sa^s\Gamma(n+2)}}_{=F(s)}ds \tag{59}$$

where $-1 < c < 0$. For future use, we define integration path $\mathcal{C}_1 = c+jx, -\infty < x < \infty$. In order to exactly

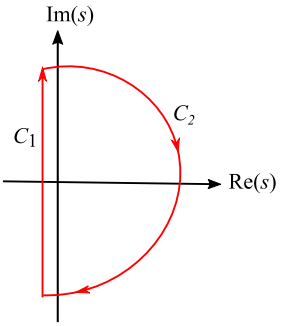

FIGURE 15. Integration contour.

evaluate (59), we use complex contour integration techniques. The following is the main tool needed. Consider that $\mathcal{C}$ is a closed curve and complex function $f(z)$ is inside and/or on $\mathcal{C}$ except for a countable number of singularities inside $\mathcal{C}$ at $z_1, z_2, \ldots$. The residue theorem establishes the value of the counter clockwise line integral of $f(z)$ over $\mathcal{C}$ as follows:

$$\frac{1}{2\pi i}\oint_{\mathcal{C}} f(z)dz = \sum_{k=1}^{n} \operatorname*{Res}_{z=z_k} f(z) \tag{60}$$

where an l-th order residue at $z = a$ is given by

$$\operatorname*{Res}_{z=a} = \lim_{z=a}\left[\frac{1}{(l-1)!}\frac{d^{l-1}}{dz^{l-1}}\left((z-a)^l f(z)\right)\right]. \tag{61}$$

To apply (60) to evaluate $I_n(a)$, we must first choose a closed contour $\mathcal{C}$. We can close the vertical integration line in (59) by an infinite radius semi-circle on the right half plane (Fig. 15). Thus, $\mathcal{C} = \mathcal{C}_1 \cup \mathcal{C}_2$ where $\mathcal{C}_2 = re^{\theta}$ with $r \to \infty$ and $-\pi/2 \le \theta \le \pi/2$. Inside $\mathcal{C}$, $F(s)$ has infinite number of poles. The residues must be summed together according to (60). However, the line integral is in clockwise direction. Thus, we have

$$I_n(a) = -\sum_{k=0}^{\infty} \operatorname*{Res}_{s=k} F(s). \tag{62}$$

Since $F(s)$ contains several $\Gamma(\cdot)$ terms, an understanding of the poles of $\Gamma(s)$ itself is warranted. By using integration by parts, we can show that $\Gamma(s) = \int_1^{\infty} t^{s-1}e^{-t}dt + \sum_{k=0}^{\infty}\frac{1}{k!(s+k)}$. This expression shows that $\Gamma(s)$ has first order poles at $s = 0, -1, -2, \ldots$. By adapting this fact, we next evaluate all the residues of $F(s)$ systematically. There are three cases to be considered:

1) **The pole at** $s = 0$. This is a second order pole. To see that, note that near $s = 0$, $F(s) \approx \frac{c\Gamma(s)}{s}$ where c is a constant. Thus, since $\Gamma(s)$ has a first-order pole at $s = 0$, $F(s)$ has a second order pole. We evaluate the residue of this pole using (61) to give

$$\operatorname*{Res}_{s=0} F(s) = -\left[\frac{\Psi(n+1)+\gamma+\ln(a)}{n+1}\right]$$

where $\Psi(z) = \frac{d}{dz}\ln\Gamma(z)$ is the Digamma function.

2) **The poles at** $s = 1, 2, \ldots, n$. These are generated from $\Gamma(1-s)$ and they do not coincide with any other poles. Hence, they are first-order poles. Thus, we evaluate this using (61) to give for $k = 1, 2, \ldots, n$,

$$\operatorname*{Res}_{s=k} F(s) = (-1)^k\left[\frac{\Gamma(k+1)\Gamma(n+1-k)}{ka^k\Gamma(n+2)}\right].$$

3) **The poles at** $s = n+1, n+2, \ldots$. These are second-order poles due to the product $\Gamma(1-s)\Gamma(n+1-s)$. We evaluate their residues using (61) as

$$\operatorname*{Res}_{s=k} F(s) = \lim_{s\to k}\frac{d}{ds}(s-k)^2 F(s) \quad k = n+1, \ldots$$

By simplifying this, we find for $k = n+1, n+2, \ldots$

$$\operatorname*{Res}_{s=k} F(s) = \frac{(-1)^n\Gamma(k)[\Psi(k)-\Psi(k-n)-\ln a]}{a^k\Gamma(k-n)\Gamma(n+2)}.$$

By adding all the residues in (62), we find

$$\begin{aligned} I_n(a) = &\left[\frac{\Psi(n+1)+\gamma+\ln(a)}{n+1}\right] \\ &+\sum_{k=1}^{n}(-1)^{k+1}\frac{\Gamma(k+1)\Gamma(n+1-k)}{ka^k\Gamma(n+2)} \\ &+(-1)^{n+1}\sum_{k=n+1}^{\infty}\frac{\Gamma(k)[\Psi(k)-\Psi(k-n)-\ln a]}{a^k\Gamma(k-n)\Gamma(n+2)}. \end{aligned} \tag{63}$$

We replace the sum index k in the second sum by $k+n+1$ and the three Gamma terms by a binomial coefficient. Thus, (63) can be further simplified as

$$\begin{aligned} I_n(a) = &\left[\frac{\Psi(n+1)+\gamma+\ln(a)}{n+1}\right] \\ &+\sum_{k=1}^{n}(-1)^{k+1}\frac{\Gamma(k+1)\Gamma(n+1-k)}{ka^k\Gamma(n+2)} + \frac{(-1)^{n+1}}{n+1} \\ &\times\sum_{k=0}^{\infty}\binom{n+k}{k}\frac{[\Psi(k+n+1)-\Psi(k+1)-\ln a]}{a^{k+n+1}}. \end{aligned} \tag{64}$$

We know that $\sum_{k=0}^{\infty}\binom{n+k}{k}x^k = \frac{1}{(1-x)^{n+1}}$ for $|x| < 1$. Thus, (64) can be further simplified as

$$\begin{aligned} I_n(a) = &\left[\frac{\sum_{k=1}^{n}\frac{1}{k}+\ln(a)}{n+1}\right] + \frac{(-1)^n}{n+1}\frac{\ln(a)}{(a-1)^{n+1}} \\ &+\sum_{k=1}^{n}(-1)^{k+1}\frac{\Gamma(k+1)\Gamma(n+1-k)}{ka^k\Gamma(n+2)} + \frac{(-1)^{n+1}}{n+1} \\ &\times\sum_{k=0}^{\infty}\binom{n+k}{k}\frac{[\Psi(k+n+1)-\Psi(k+1)]}{a^{k+n+1}}. \end{aligned} \tag{65}$$

Since $\Gamma(z+1) = z\Gamma(z)$, we have $\ln\Gamma(z+1) = \ln z + \ln\Gamma(z)$. Thus, by differentiating this, we find $\Psi(z+1) = \frac{1}{z} + \Psi(z)$. By repeatedly applying this recursion, we find that

$\Psi(k+n+1) = \Psi(k+1) + \sum_{l=1}^{n} \frac{1}{k+l}$. By using this, (65) can be further simplified as

$$I_n(a) = \left[\frac{\sum_{k=1}^{n} \frac{1}{k} + \ln(a)}{n+1}\right] + \frac{(-1)^n}{n+1}\frac{\ln(a)}{(a-1)^{n+1}} + \sum_{k=1}^{n}(-1)^{k+1}\frac{\Gamma(k+1)\Gamma(n+1-k)}{ka^k\Gamma(n+2)} + \frac{(-1)^{n+1}}{n+1}\sum_{k=0}^{\infty}\binom{n+k}{k}\frac{[\sum_{l=1}^{n}\frac{1}{k+l}]}{a^{k+n+1}}. \quad (66)$$

Note that $\frac{1}{k+l} = \int_0^1 t^{l+k-1}dt$, by substituting this in the infinite sum of (66), we find that

$$\begin{aligned}
&\sum_{k=0}^{\infty}\binom{n+k}{k}\frac{\frac{1}{k+l}}{a^{k+n+1}} \\
&= \int_0^1 t^{l-1}\sum_{k=0}^{\infty}\binom{n+k}{k}\frac{t^k}{a^{k+n+1}}dt \\
&\overset{(a)}{=} \int_0^1 \frac{t^{l-1}}{(a-t)^{n+1}}dt \\
&\overset{(b)}{=} \frac{1}{la^{n+1}}\,{}_2F_1\left(n+1, l; l+1; \frac{1}{a}\right) \\
&\overset{(c)}{=} \frac{(a-1)^{-l}}{la^{n+1-l}}{}_2F_1\left(l, l-n; l+1; \frac{1}{1-a}\right) \\
&\overset{(d)}{=} \frac{(a-1)^{-l}}{la^{n+1-l}}\sum_{j=0}^{n-l}(-1)^j\binom{n-l}{j} \times \frac{l}{(l+j)(1-a)^j} \quad (67)
\end{aligned}$$

where in (a), we used the binomial expansion for a negative integer power, (b) is obtained from [36, eq. 3.194.1], (c) is due to transformation formula for hypergeometric function [36, eq. 9.131.1], and (d) follows from the fact that the hypergeometric series ${}_2F_1(\alpha, \beta; \gamma; z)$ terminates if either α or β is a nonpositive integer: ${}_2F_1(\alpha, -m; \gamma; z) = \sum_{j=0}^{m}(-1)^j\binom{m}{j}\frac{(\alpha)_j}{(\gamma)_j}z^j$ where $(q)_j = \frac{\Gamma(q+j)}{\Gamma(q)}$ is the Pochhammer symbol. Now, by substituting (67) in (66), we get

$$I_n(a) = \left[\frac{\sum_{k=1}^{n} \frac{1}{k} + \ln(a)}{n+1}\right] + \frac{(-1)^n}{n+1}\frac{\ln(a)}{(a-1)^{n+1}} + \sum_{k=1}^{n}(-1)^{k+1}\frac{\Gamma(k+1)\Gamma(n+1-k)}{ka^k\Gamma(n+2)} + \frac{(-1)^{n+1}}{n+1}\sum_{l=1}^{n}\frac{(a-1)^{-l}}{la^{n+1-l}}\sum_{j=0}^{n-l}(-1)^j\binom{n-l}{j} \times \frac{l}{(l+j)(1-a)^j}. \quad (68)$$

Finally, substituting (68) in (57), we get (39). ■

REFERENCES

[1] Ericsson. (Nov. 2018). *Ericsson Mobility Report*. [Online]. Available: https://www.ericsson.com/assets/local/mobility-report/documents/2018/ericsson-mobility-report-november-2018.pdf

[2] T. S. Rappaport, G. R. Maccartney, M. K. Samimi, and S. Sun, "Wideband millimeter-wave propagation measurements and channel models for future wireless communication system design," *IEEE Trans. Commun.*, vol. 63, no. 9, pp. 3029–3056, Sep. 2015.

[3] T. S. Rappaport, R. W. Heath, Jr., R. C. Daniels, and J. N. Murdock, *Millimeter Wave Wireless Communications*. Upper Saddle River, NJ, USA: Prentice-Hall, 2015.

[4] S. Rangan, T. S. Rappaport, and E. Erkip, "Millimeter-wave cellular wireless networks: Potentials and challenges," *Proc. IEEE*, vol. 102, no. 3, pp. 366–385, Mar. 2014.

[5] S. Biswas, S. Vuppala, J. Xue, and T. Ratnarajah, "On the performance of relay aided millimeter wave networks," *IEEE J. Sel. Topics Signal Process.*, vol. 10, no. 3, pp. 576–588, Apr. 2016.

[6] K. Belbase, C. Tellambura, and H. Jiang, "Two-way relay selection for millimeter wave networks," *IEEE Commun. Lett.*, vol. 22, no. 1, pp. 201–204, Jan. 2018.

[7] K. Belbase, Z. Zhang, H. Jiang, and C. Tellambura, "Coverage analysis of millimeter wave decode-and-forward networks with best relay selection," *IEEE Access*, vol. 6, pp. 22670–22683, Apr. 2018.

[8] L. Kong, L. Ye, F. Wu, M. Tao, G. Chen, and A. V. Vasilakos, "Autonomous relay for millimeter-wave wireless communications," *IEEE J. Sel. Areas Commun.*, vol. 35, no. 9, pp. 2127–2136, Sep. 2017.

[9] G. Yang and M. Xiao, "Performance analysis of millimeter-wave relaying: Impacts of beamwidth and self-interference," *IEEE Trans. Commun.*, vol. 66, no. 2, pp. 589–600, Feb. 2018.

[10] T. S. Rappaport, Y. Xing, G. R. MacCartney, A. F. Molisch, E. Mellios, and J. Zhang, "Overview of millimeter wave communications for fifth-generation (5G) wireless networks—With a focus on propagation models," *IEEE Trans. Antennas Propag.*, vol. 65, no. 12, pp. 6213–6230, Dec. 2017.

[11] M. O. Hasna and M. S. Alouini, "Outage probability of multihop transmission over Nakagami fading channels," *IEEE Commun. Lett.*, vol. 7, no. 5, pp. 216–218, May 2003.

[12] S. S. Ikki and S. Aissa, "Multihop wireless relaying systems in the presence of cochannel interferences: Performance analysis and design optimization," *IEEE Trans. Veh. Technol.*, vol. 61, no. 2, pp. 566–573, Feb. 2012.

[13] V. A. Aalo, G. P. Efthymoglou, T. Soithong, M. Alwakeel, and S. Alwakeel, "Performance analysis of multi-hop amplify-and-forward relaying systems in Rayleigh fading channels with a Poisson interference field," *IEEE Trans. Wireless Commun.*, vol. 13, no. 1, pp. 24–35, Jan. 2014.

[14] G. K. Karagiannidis, "Performance bounds of multihop wireless communications with blind relays over generalized fading channels," *IEEE Trans. Wireless Commun.*, vol. 5, no. 3, pp. 498–503, Mar. 2006.

[15] T. Soithong, V. A. Aalo, G. P. Efthymoglou, and C. Chayawan, "Performance of multihop relay systems with co-channel interference in Rayleigh fading channels," *IEEE Commun. Lett.*, vol. 15, no. 8, pp. 836–838, Aug. 2011.

[16] G. Amarasuriya, C. Tellambura, and M. Ardakani, "Asymptotically-exact performance bounds of AF multi-hop relaying over Nakagami fading," *IEEE Trans. Commun.*, vol. 59, no. 4, pp. 962–967, Apr. 2011.

[17] R. Mesleh, S. S. Ikki, O. Amin, and S. Boussakta, "Analysis and optimization of AF multi-hop over Nakagami-m fading channels in the presence of CCI," in *Proc. IEEE 24th Int. Symp. PIMRC*, Sep. 2013, pp. 2021–2026.

[18] A. A. AbdelNabi, F. S. Al-Qahtani, M. Shaqfeh, S. S. Ikki, and H. M. Alnuweiri, "Performance analysis of MIMO multi-hop system with TAS/MRC in Poisson field of interferers," *IEEE Trans. Commun.*, vol. 64, no. 2, pp. 525–540, Feb. 2016.

[19] J. Qiao, L. X. Cai, and X. Shen, "Multi-hop concurrent transmission in millimeter wave WPANs with directional antenna," in *Proc. IEEE Int. Conf. Commun. (ICC)*, May 2010, pp. 1–5.

[20] J. Kim and A. F. Molisch, "Quality-aware millimeter-wave device-to-device multi-hop routing for 5G cellular networks," in *Proc. IEEE Int. Conf. Commun. (ICC)*, Jun. 2014, pp. 5251–5256.

[21] B. P. S. Sahoo, C.-H. Yao, and H.-Y. Wei, "Millimeter-wave multi-hop wireless backhauling for 5G cellular networks," in *Proc. IEEE 85th Veh. Tech. Conf. (VTC)*, Jun. 2017, pp. 1–5.

[22] J. García-Rois, F. Gómez-Cuba, M. R. Akdeniz, F. J. González-Castaño, J. C. Burguillo, S. Rangan, and B. Lorenzo, "On the analysis of scheduling in dynamic duplex multihop mmWave cellular systems," *IEEE Trans. Wireless Commun.*, vol. 14, no. 11, pp. 6028–6042, Nov. 2015.

[23] X. Lin and J. G. Andrews, "Connectivity of millimeter wave networks with multi-hop relaying," *IEEE Wireless Commun. Lett.*, vol. 4, no. 2, pp. 209–212, Apr. 2015.

[24] O. Semiari, W. Saad, M. Bennis, and Z. Dawy, "Inter-operator resource management for millimeter wave multi-hop backhaul networks," *IEEE Trans. Wireless Commun.*, vol. 16, no. 8, pp. 5258–5272, Aug. 2017.
[25] H. Miao and M. Faerber, "Self-organized multi-hop millimeter-wave backhaul network: Beam alignment and dynamic routing," in *Proc. Eur. Conf. Netw. Commun. (EuCNC)*, Paris, France, Jun. 2015, pp. 275–279.
[26] A. Chelli, K. Kansanen, M.-S. Alouini, and I. Balasingham, "On bit error probability and power optimization in multihop millimeter wave relay systems," *IEEE Access*, vol. 6, pp. 3794–3808, 2018.
[27] T. Bai and R. W. Heath, Jr., "Coverage and rate analysis for millimeter-wave cellular networks," *IEEE Trans. Wireless Commun.*, vol. 14, no. 2, pp. 1100–1114, Feb. 2015.
[28] F. E. Satterthwaite, "An approximate distribution of estimates of variance components," *Biometrics Bull.*, vol. 2, no. 6, pp. 110–114, Dec. 1946.
[29] B. L. Welch, "The generalization of 'Student's' problem when several different population variances are involved," *Biometrika*, vol. 34, nos. 1–2, pp. 28–35, Jan. 1947.
[30] H. Shokri-Ghadikolaei and C. Fischione, "Millimeter wave ad hoc networks: Noise-limited or interference-limited?" in *Proc. IEEE Globecom Workshops (GC Wkshps)*, Dec. 2015, pp. 1–7.
[31] T. Kim, J. Park, J.-Y. Seol, S. Jeong, J. Cho, and W. Roh, "Tens of Gbps support with mmWave beamforming systems for next generation communications," in *Proc. IEEE Global Commun. Conf. (GLOBECOM)*, Dec. 2013, pp. 3685–3690.
[32] T. Wang, A. Cano, G. B. Giannakis, and J. N. Laneman, "High-performance cooperative demodulation with decode-and-forward relays," *IEEE Trans. Commun.*, vol. 55, no. 7, pp. 1427–1438, Jul. 2007.
[33] W. Roh, J.-Y. Seol, J. Park, B. Lee, J. Lee, Y. Kim, J. Cho, K. Cheun, and F. Aryanfar, "Millimeter-wave beamforming as an enabling technology for 5G cellular communications: Theoretical feasibility and prototype results," *IEEE Commun. Mag.*, vol. 52, no. 2, pp. 106–113, Feb. 2014.
[34] T. Bai, R. Vaze, and R. W. Heath, Jr., "Analysis of blockage effects on urban cellular networks," *IEEE Trans. Wireless Commun.*, vol. 13, no. 9, pp. 5070–5083, Sep. 2014.
[35] E. Turgut and M. C. Gursoy, "Coverage in heterogeneous downlink millimeter wave cellular networks," *IEEE Trans. Commun.*, vol. 65, no. 10, pp. 4463–4477, Oct. 2017.
[36] I. S. Gradshteyn and I. M. Ryzhik, *Table of Integrals, Series, and Products*. New York, NY, USA: Academic, 2014.
[37] M. Abramowitz and I. A. Stegun, *Handbook of Mathematical Functions: With Formulas, Graphs, and Mathematical Tables*, vol. 55. Chelmsford, MA, USA: Courier Corporation, 1964.
[38] V. N. Q. Bao and H. Y. Kong, "Error probability performance for multi-hop decode-and-forward relaying over Rayleigh fading channels," in *Proc. 11th IEEE ICACT*, vol. 3, Feb. 2009, pp. 1512–1516.
[39] A. Annamalai, C. Tellambura, and V. K. Bhargava, "Equal-gain diversity receiver performance in wireless channels," *IEEE Trans. Commun.*, vol. 48, no. 10, pp. 1732–1745, Oct. 2000.
[40] Wolfram Research. *Mathematica Online*. Accessed: Oct. 14, 2018. [Online]. Available: https://www.wolfram.com
[41] A. Thornburg, T. Bai, and R. W. Heath, Jr., "Performance analysis of outdoor mmWave ad hoc networks," *IEEE Trans. Signal Process.*, vol. 64, no. 15, pp. 4065–4079, Aug. 2016.
[42] N. L. Johnson, S. Kotz, and N. Balakrishnan, *Continuous Univariate Distributions*, vol. 2. Hoboken, NJ, USA: Wiley, 1995.
[43] C. Tellambura, A. Annamalai, and V. K. Bhargava, "Closed form and infinite series solutions for the MGF of a dual-diversity selection combiner output in bivariate Nakagami fading," *IEEE Trans. Commun.*, vol. 51, no. 4, pp. 539–542, Apr. 2003.
[44] C. Tellambura, "Evaluation of the exact union bound for trellis-coded modulations over fading channels," *IEEE Trans. Commun.*, vol. 44, no. 12, pp. 1693–1699, Dec. 1996.
[45] *IMT Vision—Framework and Overall Objectives of the Future Development of IMT for 2020 and Beyond*, document Rec. ITU-R M.2083-0, Sep. 2015.
[46] *Part 11: Wireless LAN Medium Access Control (MAC) Physical Layer (PHY) Specifications–Amendment 3: Enhancements for Very High Throughput in the 60 GHz Band*, IEEE Standard 802.11ad, Dec. 2012.
[47] A. Annamalai, C. Tellambura, and V. K. Bhargava, "Exact evaluation of maximal-ratio and equal-gain diversity receivers for M-ary QAM on Nakagami fading channels," *IEEE Trans. Commun.*, vol. 47, no. 9, pp. 1335–1344, Sep. 1999.
[48] Y. Dhungana and C. Tellambura, "Uniform approximations for wireless performance in fading channels," *IEEE Trans. Commun.*, vol. 61, no. 11, pp. 4768–4779, Nov. 2013.

KHAGENDRA BELBASE (S'17) received the B.Eng. degree in electronics and communications engineering from the Institute of Engineering, Pulchowk Campus, Nepal, in 2010, and the M.Eng. degree from the Antenna and Radio Propagation Laboratory, Department of International Development Engineering, Tokyo Institute of Technology, Tokyo, Japan, in 2014. He is currently pursuing the Ph.D. degree with the Department of Electrical and Computer Engineering, University of Alberta, Edmonton, AB, Canada. His research interests include wireless communications theory, millimeter wave communications, wireless relaying, and the stochastic geometry analysis of wireless networks.

CHINTHA TELLAMBURA (F'11) received the B.Sc. degree (Hons.) from the University of Moratuwa, Sri Lanka, the M.Sc. degree in electronics from King's College London, U.K., and the Ph.D. degree in electrical engineering from the University of Victoria, Canada.

He was with Monash University, Australia, from 1997 to 2002. He is currently a Professor with the Department of Electrical and Computer Engineering, University of Alberta. He has authored or coauthored over 500 journal papers and conference papers with total citations over 14 000 and an h-index of 64 (Google Scholar). His current research interests include the design, modelling, and analysis of cognitive radio, heterogeneous cellular networks, and 5G wireless networks.

Prof. Tellambura he was elected as an IEEE Fellow for his contributions to physical layer wireless communication theory, in 2011. In 2017, he was elected as a Fellow of the Canadian Academy of Engineering. He was a recipient of the prestigious McCalla Professorship and the Killam Annual Professorship from the University of Alberta. He has received the Best Paper Award from the Communication Theory Symposium, in 2012, the IEEE International Conference on Communications (ICC) in Canada, and ICC 2017 in France. He has served as an Editor for the IEEE TRANSACTIONS ON COMMUNICATIONS, from 1999 to 2011 and the IEEE TRANSACTIONS ON WIRELESS COMMUNICATIONS, from 2001 to 2007. He was the Area Editor of *Wireless Communications Systems and Theory*, from 2007 to 2012.

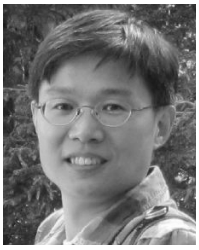

HAI JIANG (SM'15) received the B.Sc. and M.Sc. degrees in electronics engineering from Peking University, Beijing, China, in 1995 and 1998, respectively, and the Ph.D. degree in electrical engineering from the University of Waterloo, Waterloo, ON, Canada, in 2006. Since 2007, he has been a Faculty Member of the University of Alberta, Edmonton, AB, Canada, where he is currently a Professor with the Department of Electrical and Computer Engineering. His research interests include radio resource management, cognitive radio networking, and cooperative communications.